Article

Cell Reports

A Dual-Sensing Receptor Confers Robust Cellular Homeostasis

Graphical Abstract

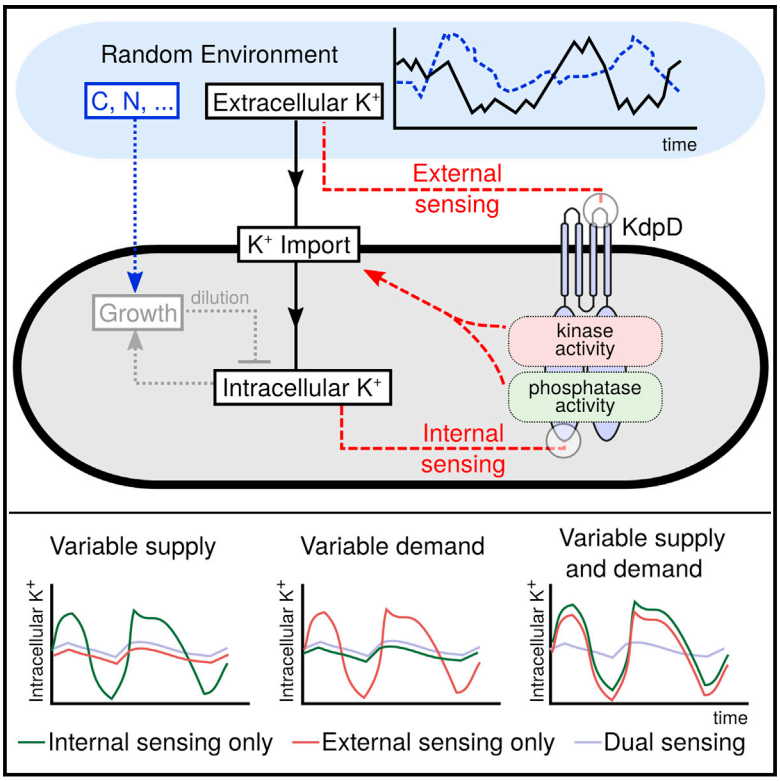

Highlights

- The bifunctional receptor KdpD senses extra- and intracellular K^+
- Kinase and phosphatase activities are regulated by K^+
- The dual-sensing strategy is superior under fluctuating conditions

Authors

Hannah Schramke, Filipe Tostevin, Ralf Heermann, Ulrich Gerland, Kirsten Jung

Correspondence

gerland@tum.de (U.G.), jung@lmu.de (K.J.)

In Brief

Schramke et al. find that the bifunctional receptor KdpD regulates its kinase and phosphatase activities by sensing extra- and intracellular K^+. Under fluctuating conditions, this dual-sensing strategy ensures robust homeostasis and outcompetes simpler strategies.

Schramke et al., 2016, Cell Reports *16*, 213–221
June 28, 2016
http://dx.doi.org/10.1016/j.celrep.2016.05.081

Cell Reports
Article

A Dual-Sensing Receptor Confers Robust Cellular Homeostasis

Hannah Schramke,[1,2,4] Filipe Tostevin,[3,4] Ralf Heermann,[2] Ulrich Gerland,[3,*] and Kirsten Jung[1,2,*]
[1]Center for Integrated Protein Science Munich (CiPSM)
[2]Department of Biology I, Microbiology
Ludwig-Maximilians-Universität München, Großhaderner Straße 2-4, 82152 Martinsried, Germany
[3]Physik Department, Technische Universität München, James Franck Straße 1, 85747 Garching, Germany
[4]Co-first author
*Correspondence: gerland@tum.de (U.G.), jung@lmu.de (K.J.)
http://dx.doi.org/10.1016/j.celrep.2016.05.081

SUMMARY

Cells have evolved diverse mechanisms that maintain intracellular homeostasis in fluctuating environments. In bacteria, control is often exerted by bifunctional receptors acting as both kinase and phosphatase to regulate gene expression, a design known to provide robustness against noise. Yet how such antagonistic enzymatic activities are balanced as a function of environmental change remains poorly understood. We find that the bifunctional receptor that regulates K^+ uptake in *Escherichia coli* is a dual sensor, which modulates its autokinase and phosphatase activities in response to both extracellular and intracellular K^+ concentration. Using mathematical modeling, we show that dual sensing is a superior strategy for ensuring homeostasis when both the supply of and demand for a limiting resource fluctuate. By engineering standards, this molecular control system displays a strikingly high degree of functional integration, providing a reference for the vast numbers of receptors for which the sensing strategy remains elusive.

INTRODUCTION

While bacteria have a limited ability to manipulate their environment, they have a remarkable capacity to adapt to changing environmental conditions while maintaining intracellular homeostasis. Two-component signaling, encompassing sensing and regulatory responses, is a major adaptation mechanism in prokaryotes. Like many control systems designed by engineers, the molecular control systems used by cells must operate under unpredictable conditions. To understand the designs that evolved in bacteria long before engineering principles were developed, we are studying the KdpD/KdpE system as a model system, one of the most widespread two-component systems in bacteria and archaea (Heermann and Jung, 2012). This system regulates K^+ homeostasis by controlling the production of the high-affinity K^+ transporter KdpFABC (Altendorf et al., 1992; Buurman et al., 2004). K^+ is the most abundant cation in all living cells, and it is crucial for the regulation of turgor and pH, as well as for the activation of several enzymes (Booth, 1985; Epstein, 2003; Nissen et al., 2000). Even though [K^+] is low in many environments, bacteria manage to maintain high intracellular K^+ concentrations. As illustrated in Figure 1A, the external availability of K^+ is expected to vary wildly, while the dilution of internal K^+ by cell growth depends on other fluctuating variables like carbon and nitrogen availability. When K^+ is abundant, the constitutive low-affinity K^+ transport systems Trk and Kup provide *Escherichia coli* cells with sufficient K^+, while KdpFABC can supply additional influx under K^+ limitation (Altendorf et al., 1992). How can a two-component system ensure optimal control of these operations under a wide variety of external and internal conditions?

The molecular architecture of the control system is illustrated in Figure 1B. The membrane-integrated receptor (sensor kinase) KdpD senses K^+ limitation, autophosphorylates, and transfers the phosphoryl group to the cytoplasmic transcriptional (response) regulator KdpE, resulting in *kdpFABC* expression. KdpD also exhibits phosphatase activity toward phospho-KdpE, which switches the signaling cascade off (Jung et al., 1997). Bifunctional enzymes acting as both autokinase and phosphatase are found in many two-component systems, and they were shown to render the response less sensitive to fluctuations in the concentrations of the two components (Batchelor and Goulian, 2003) or other factors such as ATP availability (Shinar et al., 2007). However, how the cell regulates the two enzymatic activities as a function of the sensed stimuli remains obscure.

KdpD activity is known to be modulated by K^+, since in vitro reconstruction of the KdpD/KdpE signaling cascade from purified components revealed an inhibitory effect of K^+ on KdpD-mediated phosphorylation of KdpE (Heermann et al., 2009; Lüttmann et al., 2009). However, no binding site for K^+ has ever been detected, and it is still unclear whether KdpD senses the extra- or intracellular K^+ concentration (Heermann et al., 2014; Laermann et al., 2013). Here we show that both enzymatic activities of the bifunctional receptor KdpD are directly influenced by K^+. Recognition of extracellular, periplasmic K^+ and intracellular, cytoplasmic K^+ results in the inhibition of autokinase activity and the stimulation of phosphatase activity, respectively. Mathematical modeling reveals that this dual-sensing and

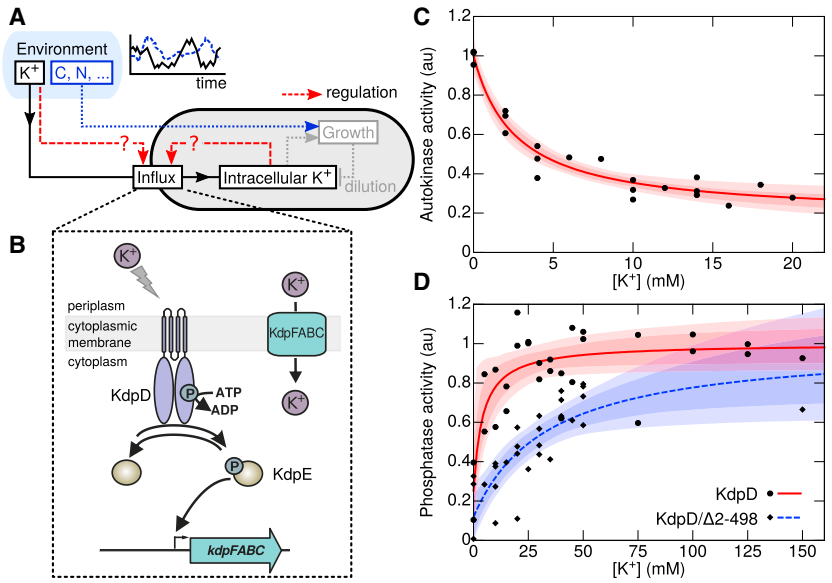

Figure 1. Sensing of K^+ by the Bifunctional Receptor KdpD

(A) Bacteria in varying environments must regulate their uptake of a limiting resource (here K^+). Uptake can be regulated in accordance with the availability of or the bacteria's need for the resource or a combination of both. Other environmental factors may non-specifically affect the demand for the resource, for example, by altering the growth rate.

(B) Schematic of the Kdp regulation system. The bifunctional receptor KdpD acts as both an autokinase (including phosphotransferase) and phosphatase for the response regulator KdpE. Phosphorylated KdpE activates expression of the genes encoding the high-affinity K^+ transporter KdpFABC.

(C and D) KdpD autokinase activity (C) and phosphatase activity (D) both depend on K^+ concentration. Autokinase activity was determined from the initial rates of KdpD autophosphorylation; phosphatase activity was determined from the initial rate of KdpE-P dephosphorylation by wild-type KdpD or by KdpD/Δ2–498. Lines show the best-fit Michaelis form; shading denotes regions that contain all activity curves within 68% and 95% confidence limits.

regulation strategy is superior for homeostasis when both the environmental supply and the demand for K^+ vary.

RESULTS

Extracellular K^+ Inhibits the Autokinase Activity and Intracellular K^+ Stimulates the Phosphatase Activity of KdpD

To analyze how K^+ affects signal transduction from KdpD to KdpE, we sought to understand how K^+ influenced the rates of each of the two enzymatic activities of KdpD (namely autokinase and phosphatase activities). It should be noted that phosphorylated KdpD immediately transfers the phosphoryl group to KdpE (phosphotransferase activity) (Jung et al., 1997). We first tested the influence of K^+ on the autokinase activity of KdpD in vitro by examining the phosphorylation of KdpD in the absence of KdpE. For these experiments, we used membrane vesicles prepared from disrupted cells. A large proportion of the vesicles produced in this way is ruptured or otherwise not sealed off, such that both the cytoplasmic and periplasmic portions of KdpD are accessible to K^+ (Mével-Ninio and Yamamoto, 1974; Zeng et al., 1998). The quantitative dependence of the autophosphorylation rate on the K^+ concentration is plotted in Figure 1C, showing that K^+ inhibits this enzymatic activity with half-maximal inhibition at $K_{0.5} = 2.7^{+1.1}_{-0.7}$ mM (upper and lower bounds of 68% confidence range).

We next studied the dependence of the KdpD phosphatase activity on K^+ by measuring the rate of dephosphorylation of phospho-KdpE in vitro in the absence of KdpD autophosphorylation. The quantitative dependence of the dephosphorylation rate on K^+ concentration is plotted in Figure 1D, and it shows half-maximal activation at $K_{0.5} = 4.2^{+7.8}_{-3.0}$ mM. K^+ therefore has both an inhibitory effect on the autokinase activity and a stimulating effect on the phosphatase activity of KdpD.

The cytoplasmic C-terminal domain of the 894-amino-acid-long KdpD, KdpD/Δ2–498 (Figure 2A), has been proposed to harbor a K^+ sensor (Rothenbücher et al., 2006). Having found that purified KdpD/Δ2–498 showed K^+-independent autokinase activity (Figure 2B), we hypothesized that this variant might have a K^+-dependent phosphatase activity. We therefore tested the effect of K^+ on the phosphatase activity of KdpD/Δ2–498 using phospho-KdpE as substrate. The quantitative dependence of the dephosphorylation rate on K^+ concentration is plotted in Figure 1D, showing a stimulatory effect with half-maximal activity at $K_{0.5} = 34^{+52}_{-19}$ mM K^+. This demonstrated that the C-terminal domain is sufficient for regulation of the phosphatase activity, but not the autokinase activity.

To search for a domain bearing a K^+ recognition site, we tested the K^+-dependent autokinase activity of several truncated KdpD proteins. The input domain of KdpD consists of the conserved KdpD domain, the Usp domain, four transmembrane helices, and the GAF domain (Heermann and Jung, 2012) (Figure 2A). Remarkably, the autokinase activity of a truncated KdpD variant that lacked the Kdp and Usp domains but still retained the four transmembrane helices (KdpD/Δ12–395, Figure 2) displayed a K^+ sensitivity similar to that of wild-type KdpD. Therefore, we focused on a stretch of conserved amino acids in the second periplasmic loop (loop 3) (Figure 3A), and we employed a systematic alanine mutagenesis screen. Using an *E. coli* $P_{kdpFABC}$::*lacZ* reporter strain, we found that KdpD variants with alanine substitutions at amino acid positions Pro466, Thr469, Leu470, and Val472 were less K^+ sensitive and that these mutations shifted the onset of *kdpFABC* expression to external K^+ concentrations that would normally inhibit expression (Figure 3B).

Finally, we generated a KdpD variant in which all four of these amino acids were replaced with alanine and designated this variant as $KdpD^1$ (Figure 4A). $KdpD^1$ was characterized by a K^+-independent autokinase activity and a K^+-sensitive phosphatase activity for KdpE-P in vitro (Figure 4B). The regulation of the phosphatase activity was found to be similar to the C-terminal KdpD/Δ2–498 fragment ($K_{0.5} = 32^{+71}_{-18}$ mM K^+; Figure S1). Further evidence for K^+ recognition by the second periplasmic loop was

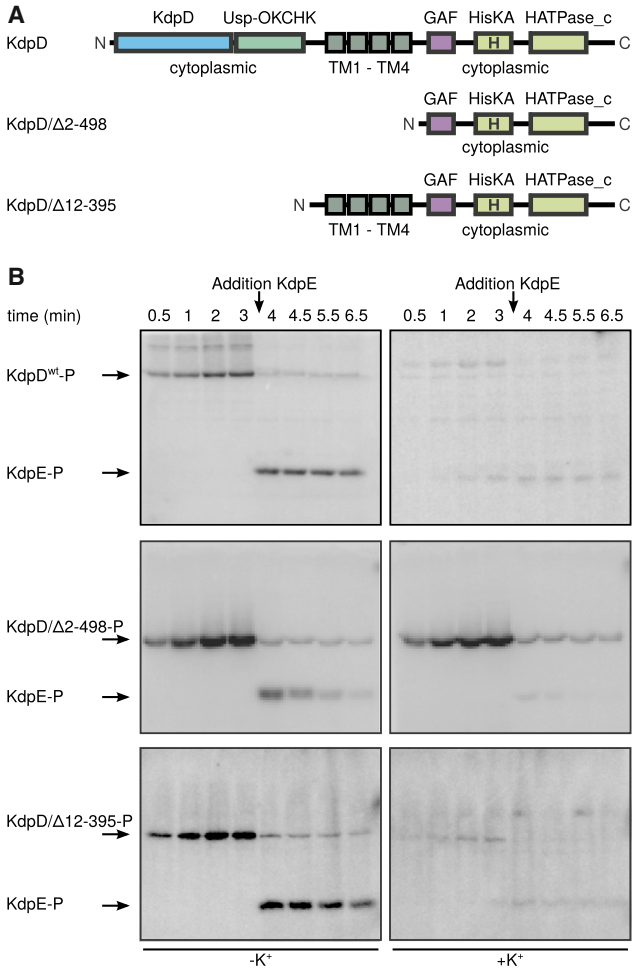

Figure 2. In Vitro Activities of Truncated KdpD Variants

(A) Schematics show wild-type KdpD in comparison to the truncated variants KdpD/Δ2–498 and KdpD/Δ12–395. TM, transmembrane helix.

(B) Time-dependent autophosphorylation of KdpD and truncated KdpD variants and dephosphorylation of KdpE in the absence (–) and presence (+) of 250 mM K^+ at constant ionic strength. Shown are representative autoradiographs of three independent experiments.

provided by variants in which the N- and C-terminal cytoplasmic domains of KdpD were connected by different linkers. When the two domains were connected by a 5Gly/5Ala or a 10Gly linker, *kdpFABC* expression in the reporter strain was no longer repressed at high [K^+]; however, when the domains were linked by the periplasmic loop sequence, repression at high [K^+] was restored (Figure S2). Together, these data suggest that the second periplasmic loop of KdpD contains a specific K^+ recognition site that regulates autokinase activity in response to extracellular K^+.

We next turned to the K^+-dependent regulation of the phosphatase activity. As mentioned above, the C-terminal cytoplasmic domain of KdpD has a K^+-dependent phosphatase activity (Figure 1D). However, in spite of intensive efforts, we could not localize a K^+ recognition site in this domain. In an attempt to circumvent this difficulty, we asked whether loss of the phosphatase activity affected the K^+ dependence of the autokinase activity. Amino acid substitutions at position Thr677 in KdpD are known to eliminate the phosphatase activity (Figure 4A) (Brandon et al., 2000), as do substitutions of the same conserved threonine residue in many other sensor kinases (Willett and Kirby, 2012). We therefore assayed the activity of the KdpD variant Thr677→Ala ($KdpD^2$) in vitro. The data revealed that, although $KdpD^2$ lacked phosphatase activity, it retained K^+-sensitive autokinase activity (Figure 4B). Thus, how exactly K^+ modulates the phosphatase activity of KdpD remains unclear; it may act via the cytoplasmic GAF domain (residues 515–655), since GAF domains are well-known ligand-binding sites also for ions (Cann, 2007a, 2007b; Heikaus et al., 2009). However, our data clearly demonstrate that the autokinase and phosphatase activities of KdpD are individually regulated by K^+.

Next we combined the mutations of *kdpD*^{1} and *kdpD*^{2}, and we found that the resulting $KdpD^{1+2}$ variant had an additive phenotype, displaying a K^+-independent autokinase activity and no phosphatase activity such that KdpE remained stably phosphorylated (Figure 4B). Taken together, these results support the idea that KdpD senses extracellular K^+ via the periplasmic loop to control its autokinase activity, while intracellular K^+ boosts its phosphatase activity.

Regulation of Both Enzymatic Activities Is Essential for a Controlled Stress Response

To probe the functional behavior of the Kdp system in vivo, we shifted exponentially growing *E. coli* MG1655 cells from K^+-saturating conditions to media that imposed different degrees of K^+ limitation, and we monitored extra- and intracellular K^+ levels and growth over time (Figure 5B; Figure S3). The cells maintained K^+ homeostasis until extracellular K^+ was completely exhausted, but they continued to grow beyond this point, thus progressively diluting their intracellular pool of K^+. The decrease in intracellular [K^+] was in turn accompanied by a gradual reduction in the growth rate of the population. We then probed the response mediated by wild-type KdpD as well as that of variants $KdpD^1$, $KdpD^2$, and $KdpD^{1+2}$ by quantifying the production of the high-affinity transporter KdpFABC 2 hr after shifting cells to media with different K^+ concentrations covering a broad range of K^+ availability (Figure 5C). Wild-type KdpD mediated a graded KdpFABC response at external K^+ concentrations below 5 mM. The $KdpD^1$ variant displayed this behavior only at very low K^+ concentrations, such that KdpFABC was produced at a constant rate at [K^+] > 1 mM, which was consistent with its K^+-independent autokinase activity. The $KdpD^2$ variant was less sensitive to intracellular K^+ than the wild-type, highlighting the importance of the counteracting phosphatase activity in ensuring a tightly controlled stress response. Finally, in cells harboring the $KdpD^{1+2}$ variant, KdpFABC production became essentially independent of [K^+]. Similar results were obtained on the basis of $P_{kdpFABC}$::*lacZ* promoter activity (Figure 3C).

A Mathematical Model Describes the In Vivo Response Dynamics

To quantitatively explore the consequences of different regulatory strategies, we developed a mathematical model for the relevant aspects of the Kdp system, including the dynamics of

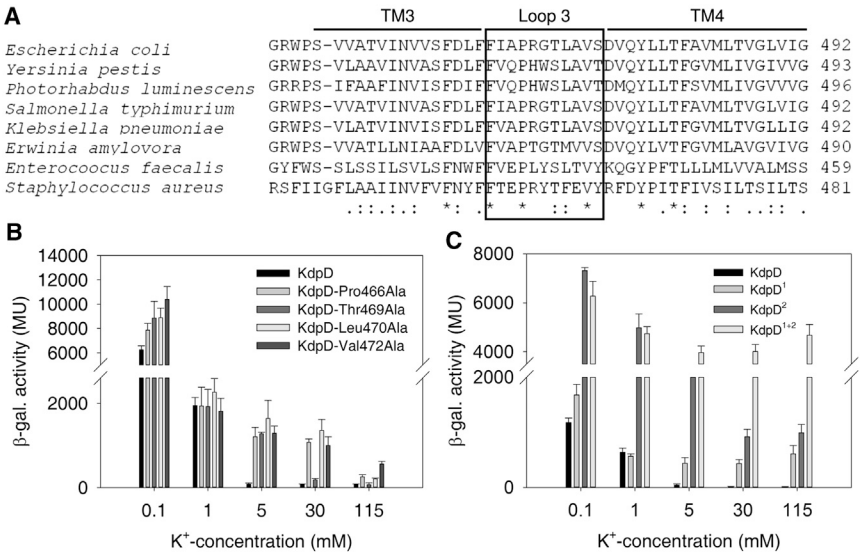

Figure 3. The Periplasmic Loop between Transmembrane Helix Three and Four Is Involved in K^+ Sensing

(A) Multiple sequence alignment of the periplasmic loop (loop 3) between transmembrane helix 3 (TM3) and helix 4 (TM4). The alignment was created using the ClustalW2 program (Goujon et al., 2010). Protein sequences were as follows: *E. coli*, UniProt: P21865; *Y. pestis*, UniProt: Q7CJR5; *P. luminescens*, UniProt: B6VN55; *S. typhimurium*, UniProt: A0A0D6H090; *K. pneumoniae*, UniProt: B5XZF1; *E. amylovora*, UniProt: D4I3U7; *E. faecalis*, UniProt: Q838F4; and *S. aureus*, UniProt: A0A0H2XIE2.

(B) The β-galactosidase activities of the reporter strain ($P_{kdpFABC}$::*lacZ*) carrying plasmids encoding KdpD and the variants KdpD-Pro466Ala, KdpD-Thr469Ala, KdpD-Leu470Ala, and KdpD-Val472Ala were determined after cultivation of cells in minimal medium at the indicated K^+ concentrations.

(C) The β-galactosidase activities of the reporter strains LF3, HS2, HS3, and HS4 ($P_{kdpFABC}$::*lacZ*) carrying KdpD and the variants $KdpD^1$, $KdpD^2$, and $KdpD^{1+2}$ were determined after cultivation of cells in minimal medium at the indicated K^+ concentrations.

KdpD/KdpE phosphorylation, rates of KdpFABC production and turnover, rates of K^+ import by both KdpFABC and constitutive transporters, and K^+-dependent growth (see the Supplemental Experimental Procedures for details). While previous models were forced to make ad hoc assumptions about the regulation of the Kdp response (Heermann et al., 2014), we used the enzymatic activities measured in vitro (Figures 1C and 1D) to parameterize the effects of both extracellular and intracellular K^+ on KdpD.

Structural data for bifunctional sensor kinases have suggested the existence of distinct conformational states that possess either autokinase or phosphatase activity (Marina et al., 2005; Ferris et al., 2012; Huynh and Stewart, 2011). Our observation that $KdpD^1$ possesses K^+-independent autokinase activity but retains K^+-sensitive phosphatase activity is inconsistent with a simple two-state model in which KdpD is always either autokinase or phosphatase active, which implies that the two activities must always be anti-correlated. We therefore considered an extension of this model consisting of three distinct conformational states of KdpD, corresponding to autokinase-active, phosphatase-active, and inactive conformations (Figure 5A). Switching among these states was assumed to obey thermodynamic equilibrium statistics (Bhate et al., 2015), with switching constants that vary depending on the extra- and intracellular concentrations of K^+. In such a model, the autokinase and phosphatase activities are correlated and both depend on extra- and intracellular K^+. The parameters of these switching constants were determined by fitting to the in vitro enzymatic activities of wild-type KdpD and the $KdpD^1$ variant (Figures 1C and 1D; Figure S1), assuming that the observed activity is proportional to the fraction of KdpD molecules in the corresponding conformational state.

The resulting parameterized switching model was then used as the input into a coarse-grained description of KdpD/KdpE signaling and response via *kdpFABC* expression. Parameters for this larger model were taken from the literature where possible or otherwise fit to experimental data. The model was able to reproduce both the phosphorylation dynamics in vitro (Figure S4) and the in vivo response (Figures 5B and 5C, lines) for wild-type KdpD and the variants $KdpD^1$, $KdpD^2$, and $KdpD^{1+2}$, showing that our regulation model is able to capture the main features of KdpD/KdpE signal transduction.

Dual Sensing by a Bifunctional Receptor Ensures Robust Homeostasis in Fluctuating Environments

We next sought to compare the performance of cells employing the dual-sensing strategy to that of mutants with only internal or external sensing under conditions of unpredictable environments (illustrated in Figure 1A). The strains carrying *kdpD*^{1} and *kdpD*^{2} mutations were unsuited for this purpose, since these cells constitutively produce high levels of the K^+ transporter. We therefore employed our model to compare the following three alternative regulation strategies (Figure 6A): (1) the DUAL strategy of wild-type KdpD featuring dual-sensing and bifunctional activities, as revealed by our experiments; (2) external sensing (EX) only, where the enzymatic activities of KdpD are dependent on extracellular K^+ but are insensitive to changes in intracellular K^+; and (3) internal sensing (IN) only, where the enzymatic activities of KdpD are responsive to intracellular, but not extracellular, K^+.

We first asked how accurately each strategy was able to regulate the K^+ uptake flux in response to varying K^+ supply by comparing steady-state intracellular K^+ levels across a range of extracellular K^+ concentrations (Figure S5A). The DUAL strategy showed less variability than the IN strategy, which can trigger K^+ uptake only after intracellular $[K^+]$ has changed. However, the differences between the DUAL and EX strategies were small, indicating that the additional feedback from intracellular K^+ to uptake plays little role under constant conditions.

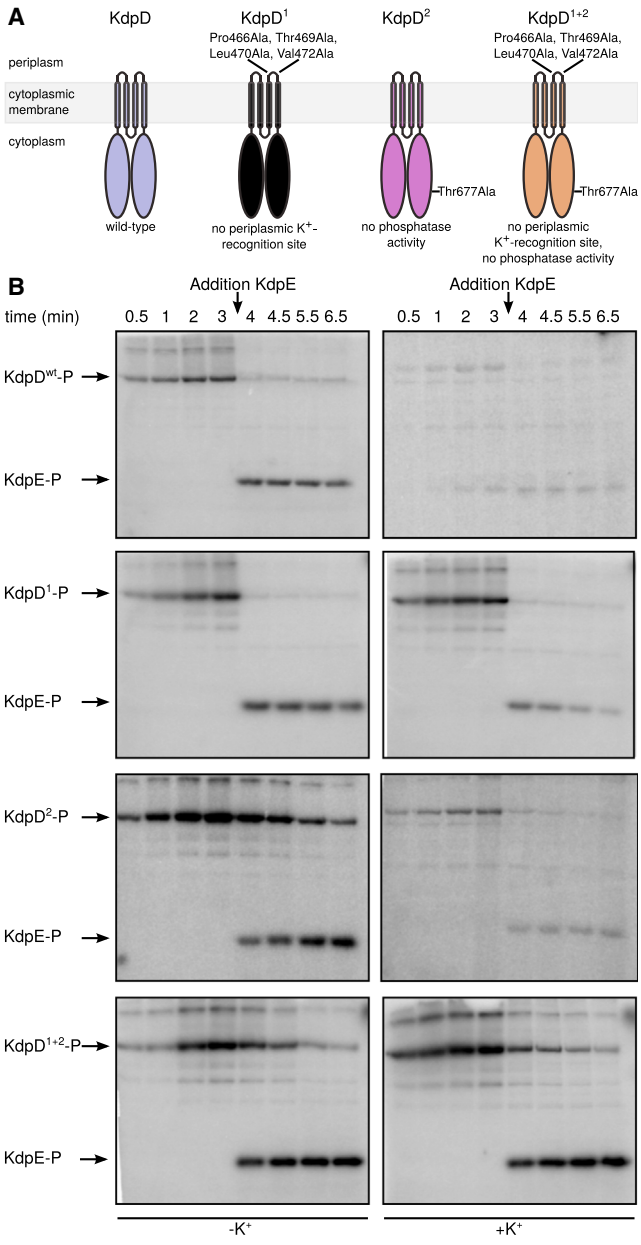

Figure 4. KdpD Senses Extracellular and Intracellular K^+

(A) Topology model of wild-type KdpD and the locations of amino acid substitutions. Variant $KdpD^1$ contains four amino acid substitutions (Pro466→Ala, Thr469→Ala, Leu470→Ala, and Val472→Ala) in the periplasmic loop region. $KdpD^2$ contains a single substitution (Thr677→Ala) in the C-terminal domain. $KdpD^{1+2}$ combines these five substitutions.

(B) Time-dependent autokinase activity of KdpD and KdpD variants in membrane vesicles was monitored by incubation with [γ-^{32}P]ATP in the presence and absence of K^+. After 3.5 min, KdpE was added and phosphotransfer and time-dependent dephosphorylation were monitored. Phosphorylated KdpD and KdpE were separated by SDS-PAGE and gels were exposed to a phosphoscreen. Due to the use of membrane vesicles, a number of unspecific bands are detectable, as, for example, seen in the top right picture, in which KdpD autokinase activity is completely inhibited by K^+. See Figure S6 for plots of the phosphorylation time courses, as obtained by quantification of the band intensities.

We reasoned that internal sensing could be beneficial if the intracellular K^+ level were to change independently of the extracellular environment. Crucially, the intracellular K^+ concentration depends on both the uptake rate and the rate of dilution due to growth (Figure 6B). If cells were exposed to environmental fluctuations that affected growth in a K^+-independent manner (e.g., changing carbon or nitrogen availability), the intracellular K^+ concentration would be altered even though the environmental K^+ level was unchanged. We therefore simulated direct competition among the strategies, which differ only in the regulation of KdpD activity as a function of K^+ level, under conditions of fluctuating K^+ supply and fluctuations in the maximal growth rate (Figure 6B). In our model the instantaneous growth rate is taken to be a monotonic, saturating function of the intracellular K^+ concentration, with a prefactor determined by the environment; thus, differences in the growth rate among strategies reflect differences in intracellular K^+ depletion. We found that both the EX and IN strategies were outcompeted by the DUAL strategy, which ultimately came to dominate the population (Figure 6C). The poor performance of the EX strategy in this competition was primarily due to its inability to respond to the increasing demand for K^+ under conditions of rapid growth. This dominance of dual sensing over internal sensing is due to its ability to achieve K^+ homeostasis more reliably (Figure S6B), as also was observed in the constant environments. The advantage of the DUAL strategy may in fact be greater than estimated here, as our model does not include any penalty for the superfluous overproduction of KdpFABC in high [K^+] environments.

DISCUSSION

Conservation of crucial resources in fluctuating environments is particularly challenging for unicellular organisms. Under K^+-limiting conditions, induction of *kdpFABC* expression is controlled by the bifunctional sensor kinase KdpD via KdpE, which ultimately leads to production of the high-affinity KdpFABC transport system (Figures 1A and 1B). In this study, we show that KdpD is able to monitor concentrations of both extra- and intracellular K^+ and to regulate its dual function as an autokinase and a KdpE-specific phosphatase, according to the K^+ concentrations of the two K^+ pools (Figures 1C and 1D). The observed $K_{0.5}$ value for autokinase activity is in the range of environmental K^+ concentrations at which induction is observed in vivo, and amino acid replacements in the periplasmic loop of KdpD lead to loss of its sensitivity to external K^+. Furthermore, we demonstrated that the phosphatase activity is stimulated by intracellular K^+ via a sensor module located in the C-terminal cytoplasmic domain of KdpD (Figures 1, 2, and 4), although we cannot rule out additional regulation of phosphatase activity by extracellular K^+.

These results led us to formulate a dual-sensing, dual-regulation model for K^+-dependent KdpD signaling (Figure 5A), which reproduces the basic features of the system (Figures 5B and 5C). When the extracellular K^+ concentration is high (>5 mM), K^+ is recognized by the periplasmic loop and inhibits the autokinase activity. At the same time intracellular K^+ is sensed by the C-terminal cytoplasmic domain and stimulates the phosphatase activity. Consequently, KdpD acts as a phosphatase on KdpE-P,

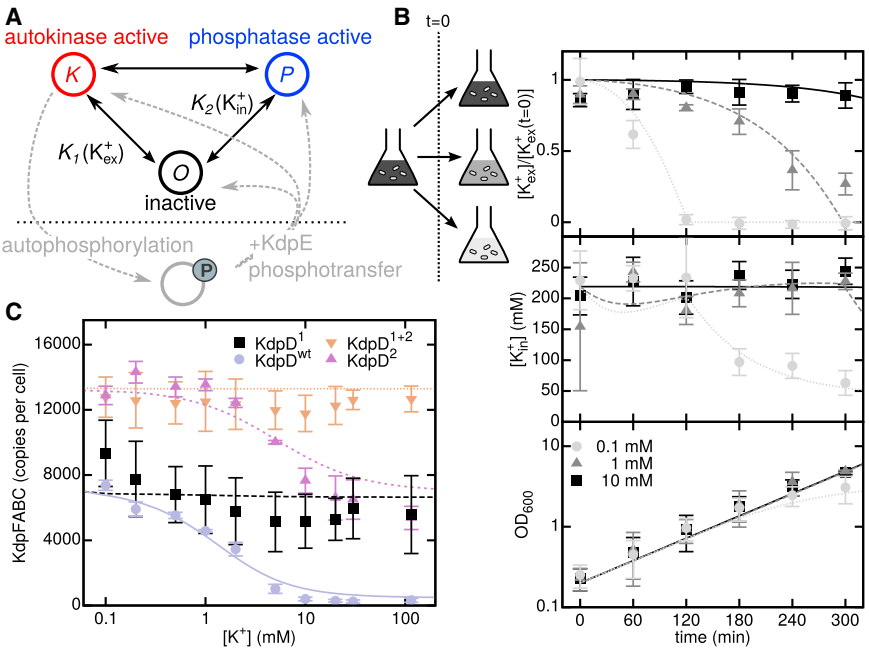

Figure 5. Dynamics of Kdp Response In Vivo

(A) Schematic of switching model of KdpD enzymatic activity. Autokinase and phosphatase activities are assumed to correspond to two distinct molecular conformations, *K* and *P*. A third inactive conformation, *O*, has no enzymatic activity. The equilibrium occupancy of each conformation is biased according to the extracellular and intracellular K^+ concentrations. Molecules in the *K* state can undergo autophosphorylation. Subsequently, phosphotransfer from phospho-KdpD to KdpE returns KdpD to each state according to their equilibrium occupancies.

(B) Dynamics of intracellular and extracellular K^+ concentrations for wild-type cells measured by atomic absorption spectroscopy and optical density at 600 nm. At time t = 0, cells were transferred from medium containing 10 mM K^+ to media with the indicated concentrations.

(C) KdpFABC levels were determined by quantitative western blot analysis, 120 min after transfer of cells to media with the indicated K^+ concentration. Data points are the mean ± SD of three biological replicates. Lines show results of the mathematical model.

and production of the high-affinity K^+ transporter is prevented. When environmental levels of K^+ fall below the threshold for autokinase activation, *kdpFABC* expression is initiated; however, as long as the intracellular K^+ concentration remains high, the KdpD phosphatase activity remains stimulated. Under these conditions, the intracellular response is attenuated for as long as the high intracellular K^+ concentration is sufficient for all cellular processes. The longer the cells are exposed to K^+ limitation or extreme K^+ limitation, the greater the drop in intracellular [K^+]. Eventually, the phosphatase activity is no longer stimulated and higher amounts of KdpE become phosphorylated, resulting in maximal production of KdpFABC.

Importantly, this dual-sensing, dual-regulation mechanism allows *E. coli* not only to respond to impending limitation by sensing the extracellular K^+ concentration but also to regulate the activation level in response to changing intracellular K^+ requirements. In particular, the demand for K^+ is determined by the cellular growth rate. In media that permit rapid growth, intracellular K^+ could become depleted even though it is abundant in the environment. Under these conditions, sensing of the intracellular K^+ level allows the cell to fine-tune its uptake rate to match the demand. We included this cellular scenario in our mathematical model, and we used simulations to compare the dual-sensing strategy to strategies with sensing of only one K^+ pool under variation of both environmental [K^+] and growth rate. We found that the dual-sensing strategy was better able to maintain intracellular [K^+] within the tolerable range, and, therefore, it was able to outcompete single-sensing strategies (Figure 6). The same regulatory dynamics can account for the induction of *kdpFABC* expression under other conditions that reduce the availability of free intracellular K^+, such as extracellular Cs^+ or low pH (Jung et al., 2001; Roe et al., 2000).

Dual sensing thus emerges as a highly optimized regulation strategy. The key advantage of this strategy is the ability to directly sense changes in both supply of and demand for the limiting resource. It is in fact analogous to strategies that are widely used in control engineering (Kilian, 2005). For example, temperature controllers often monitor both internal and external temperatures to control heating and cooling elements (Figure 7). In this case, dual sensing keeps room temperature constant in the face of unpredictable changes in the weather or when variables such as incident sunlight, room occupancy, or the opening of doors affect heat influx and leakage. However, whereas engineered control systems usually have separate sensors, controllers, and actuators, bacteria have found a remarkably compact and integrated solution in the case of the Kdp system, with KdpD providing the functions of the sensors, the controller, and, aided by KdpE, also the actuator (Figure 7). Combining dual sensing with sensor kinase bifunctionality increases the reliability of homeostasis by ensuring robustness to changes in the protein concentrations (Batchelor and Goulian, 2003; Shinar et al., 2007). Dual sensing could, in principle, also be implemented by integrating both signals to regulate only one enzymatic activity. However, the regulation of both activities, as we observed for KdpD, may provide additional advantages, such as increasing the dynamic range of signaling.

Our data do not identify the specific molecular transitions that determine the catalytic activities of KdpD, although we suggest that KdpD integrates distinct K^+ signals from at least two sensory domains. Structural data for conserved sensor kinase domains support the existence of distinct conformational states of bifunctional sensor kinases with autokinase or phosphatase activity (Marina et al., 2005; Ferris et al., 2012; Huynh and Stewart, 2011). Here we have used the simplest generalization of this conformational model to incorporate a third, enzymatically inactive state. However, the multidomain structure of KdpD potentially allows for a far larger number of conformations, as each domain may respond differently in the presence of distinct

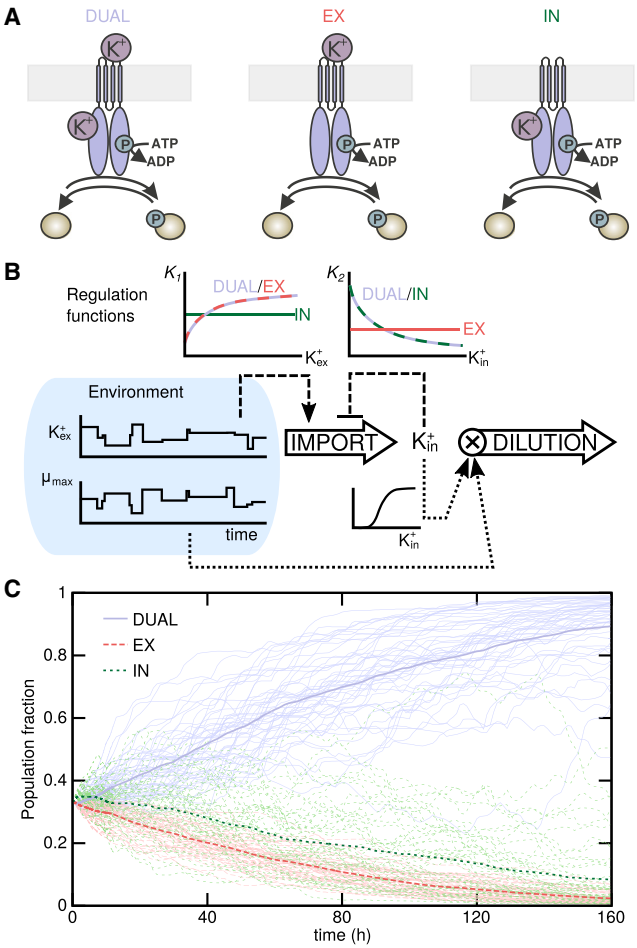

Figure 6. Dual Sensing and Dual Regulation Provide Robust Control of Intracellular K^+

(A) Illustrations show the three different regulation strategies. DUAL strategy, KdpD autokinase activity and phosphatase activity are regulated by both extracellular and intracellular K^+; EX strategy, both activities are regulated by extracellular K^+ independently of intracellular K^+; IN strategy, both activities are regulated by intracellular K^+ independently of extracellular K^+.

(B) Each strategy is characterized by the regulation functions that determine the enzymatic activities of KdpD as a function of the intra- and extracellular K^+. These control, via *kdpFABC* expression, the K^+ import rate. The rate of dilution of intracellular K^+ is the instantaneous growth rate, which is taken to be the product of the environmentally determined maximal growth rate, μ_{max}, and a factor that depends on the intracellular K^+ level. Both μ_{max} and the environmental K^+ level are subject to fluctuations over time.

(C) Simulations of the outcome of competition among the three strategies. Starting from initially equal numbers of cells implementing each strategy, the plots depict the evolutionary trajectories of the subpopulations in environments in which both the extracellular K^+ supply and the maximal growth rate vary. Light lines show results for individual environmental realizations and thick lines show the mean over 50 realizations.

stimuli (Bhate et al., 2015). It therefore remains to be determined precisely how the dual K^+ stimuli are encoded in KdpD dynamics at a molecular scale.

The combination of extra- and intracellular sensing has been shown previously for Mg^{2+} homeostasis in the pathogen *Salmonella enterica* serovar Typhimurium, albeit via a very different

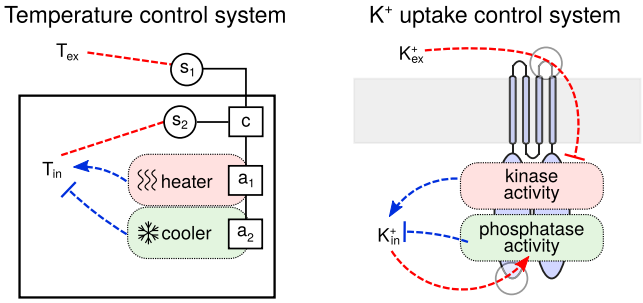

Figure 7. Schematic Comparison of a Temperature Control System with KdpD

A temperature controller (c) integrates measurements of the internal and external temperatures from individual sensors (s) into signals that regulate the actuators (a) of a heater and a cooler. KdpD is an all-in-one control system for K^+ uptake: it combines extracellular and intracellular sensing functions, which control its autokinase and phosphatase activities, respectively, as well as the actuators of the downstream pathway.

mechanism. The PhoP/PhoQ two-component system in *Salmonella* senses external Mg^{2+} limitation to activate target gene expression (García Véscovi et al., 1996). In addition, transcription of the gene encoding the Mg^{2+} transporter MgtA is influenced by intracellular Mg^{2+}. More precisely intracellular Mg^{2+} binds to the *mgtA* 5′ UTR and terminates transcription via stem-loop formation (Cromie et al., 2006). The expression of *mgtA* is thus regulated by both the intra- and extracellular Mg^{2+} concentrations. However, unlike the Kdp system, the two signals are not integrated at the level of the sensor kinase; instead, they act at different levels of the response pathway. Such different regulation mechanisms may have specific functional implications. For example, post-transcriptional regulation of transporters would allow for a faster response than can be achieved by transcriptional regulation, providing better adaptation to rapidly varying signals or limiting over-accumulation if resources suddenly become abundant after limitation. Indeed, it is likely that the Kdp system is not only controlled at the transcriptional level but also at the post-translational level by proteolysis (Heermann et al., 2014) and modulation of KdpFABC activity at high K^+ concentrations (Roe et al., 2000; Damnjanovic and Apell, 2014). For most signal transduction pathways, the precise signaling mechanism has remained elusive up to now, and it is conceivable that dual sensing by bifunctional receptors and other similarly elaborate mechanisms that integrate multiple signals is the rule rather than the exception.

EXPERIMENTAL PROCEDURES

Strains and Plasmids

All strains used in this study are listed in Table S1, oligonucleotides are listed in Table S2, and plasmids are listed in Table S3. For details of strain and plasmid construction, see the Supplemental Experimental Procedures.

Phosphorylation and Dephosphorylation Assays

Membrane vesicles (see the Supplemental Experimental Procedures) containing ~0.2 mg/ml KdpD were incubated in phosphorylation buffer (50 mM Tris/HCl [pH 7.5], 10% glycerol [v/v], 0.5 M NaCl, 10 mM $MgCl_2$, and 2 mM DTT) at room temperature. Phosphorylation was initiated by the addition of 20 μM [γ-^{32}P]ATP (2.38 Ci/mmol). At different times, aliquots were removed and the

reaction was stopped by mixing with SDS sample buffer (Jung et al., 1997). After incubation for 3.5 min, purified KdpE (see the Supplemental Experimental Procedures) was added at a final concentration of 0.1 mg/ml to the KdpD-containing samples (resulting in a 1:2 dilution of KdpD, ATP, and K^+ concentration) and the incubation was continued. Additional aliquots were removed at different times and mixed with SDS sample buffer.

For dephosphorylation assays, 10His-KdpE-^{32}P was obtained as described (Jung and Altendorf, 1998). Dephosphorylation was initiated by the addition of membrane vesicles containing ~0.1 mg/ml of either KdpD or the purified C-terminal cytoplasmic domain KdpD/Δ2–498 (0.1 mg/ml), 20 mM $MgCl_2$ in the presence of 20 μM ATP-γ-S. To test for K^+-dependent dephosphorylation of KdpE, we added KCl at the indicated concentrations. In both assays the ionic strength was always kept constant at 0.5 M by supplementing with NaCl (Jung et al., 1997). At different times, aliquots were removed and the reaction was stopped by the addition of SDS sample buffer. All samples were immediately subjected to SDS-PAGE. Shortly before the end of electrophoresis, an [γ-^{32}P] ATP standard was loaded onto the gels. Gels were then dried and protein phosphorylation was detected by exposure of the gels to a Storage Phosphor Screen. Phosphorylated proteins were quantified by image analysis using Image Quant® software (GE Healthcare).

Determination of Extracellular and Intracellular K^+ Concentrations

K^+ concentrations were determined by atomic absorption spectroscopy (Bossemeyer et al., 1989). Briefly, *E. coli* MG1655 (Table S1) was cultivated in minimal medium containing 10 mM K^+ (Epstein and Kim, 1971). Cells were collected by centrifugation and transferred into pre-warmed minimal medium containing 0.1, 1, and 10 mM K^+, respectively, and then incubated aerobically at 37°C for 2 hr. Aliquots (1 ml) were taken and centrifuged through 200 μl silicone oil (DC550) at 13,000 rpm for 2 min. The K^+ content of the cell pellets and the supernatants was then determined in an atomic absorption spectrometer (Varian AA240 Spectroscopy Instrument, Agilent Technologies). To determine the fraction of bound and freely diffusible K^+, 0.5-ml samples were collected and diluted in either 0.5 ml medium (total K^+) or 0.5 ml $_{dd}H_2O$ (bound K^+) (Bossemeyer et al., 1989). After centrifugation through silicone oil, the K^+ content of the cell pellets was determined by atomic absorption spectroscopy. The fraction of free K^+ is defined as the difference between the total K^+ content and the bound K^+ content. The intracellular concentrations were calculated by taking the number of cells per sample and the cytoplasmic volumes into account. Since it has been shown that cell volumes remain more or less constant during the experiments, an average value of 8.12×10^{-16} l per cell was used in all calculations (Heermann et al., 2014).

Determination of $P_{kdpFABC}$ Activity In Vivo

In vivo signal transduction was probed using *E. coli* strain HAK006 (Table S1) transformed with plasmids carrying *kdpD* or the corresponding variants (Table S3), as previously described (Epstein and Kim, 1971; Miller, 1992). Cells were grown in minimal medium containing different K^+ concentrations (Epstein and Kim, 1971) and harvested in the mid-exponential growth phase by centrifugation. β-Galactosidase activity was determined as described (Miller, 1992) and is given in Miller units. Strains carrying mutations *kdpD*^{1}, *kdpD*^{2}, and *kdpD*$^{1+2}$ (HS2, HS3, and HS4) (Table S1) were aerobically cultivated in minimal medium containing 5 mM K^+ at 37°C until OD_{600} = 0.5, then they were shifted to minimal media containing different K^+ concentrations for 2 hr. After harvesting the cells, β-galactosidase activity was determined as described before (Miller, 1992).

Determination of KdpFABC Production by Quantitative Western Blot Analysis

Levels of KdpFABC in *E. coli* strains were determined by quantitative western blot analysis. *E. coli* strains LF3, HS2, HS3, and HS4 (Table S1) were grown aerobically at 37°C to OD_{600} = 0.5 in minimal media containing 10 mM K^+ (Epstein and Kim, 1971). Then the cells were shifted to minimal medium containing the indicated K^+ concentrations. After 2 hr the OD_{600} was adjusted to 1 and aliquots of the cultures were collected by centrifugation. Cells were resuspended in SDS sample buffer and subjected to SDS-PAGE. Proteins were electroblotted onto a nitrocellulose membrane, and the blots were blocked with 5% (w/v) skim milk in buffer A (10 mM Tris/HCl [pH 7.4] and 0.15 M NaCl) for 1 hr. Anti-KdpB antibody (Heermann et al., 2009) was added at a final dilution of 1:10,000 and incubation was continued for 1 hr. After washing with buffer A, goat anti-rabbit IgG conjugated with alkaline phosphatase was added in a final dilution of 1:2,500, and incubation was continued for 1 hr. After washing thoroughly, blots were developed with substrate solution (50 mM Na_2CO_3 [pH 9.5], 0.01% [w/v] nitro-blue-tetrazolium, and 5 mg/ml 5-bromo-4-chloro-3-indolylphosphate). Blots were scanned at high resolution in 256 gray scales, imported as TIF files into ImageJ, and the amount of KdpB was quantified. For each biological replicate, we calibrated the mean of two technical replicates using previously measured molecule numbers (Heermann et al., 2014), by finding a linear scaling coefficient that minimized the total squared deviation for the wild-type strain at the K^+ concentrations for which measurements were available in both datasets. The scaling coefficient was applied to all samples on a given blot. Data represent the average values and SD of three independent biological replicates.

Fitting of Autokinase and Phosphatase K^+ Dependency

To determine the initial reaction rate, samples were taken after 10 and 20 s for the autokinase activity and after 1 and 2 min to determine K^+-dependent dephosphorylation of KdpE. This slope was used as a measure of the enzymatic activity. To minimize day-to-day variability, the activities in each replicate dataset were scaled by a constant factor, chosen to minimize the mean-squared deviation among all datasets (three independent experiments for autokinase activity of wild-type KdpD; two independent experiments each for phosphatase activity of wild-type KdpD, KdpD/Δ2–498, and KdpD^1). The different datasets were then pooled, and non-linear least-squares fitting was performed on the pooled data via the Levenberg-Marquardt method. For autokinase activity of wild-type KdpD a model of the form $c_1 + c_2(K_{0.5}/([K^+] + K_{0.5}))$ was assumed. The resulting best-fit parameter values were c_1 = 0.18 a.u., c_2 = 0.82 a.u., and $K_{0.5}$ = 2.7 mM. A model of the form $c_1 + c_2([K^+]/([K^+] + K_{0.5}))$ was used for fitting of the phosphatase activity. Best-fit parameter values were as follows: for wild-type KdpD: c_1 = 0.25 a.u., c_2 = 0.75 a.u., and $K_{0.5}$ = 4.2 mM; for KdpD/Δ2–498: c_1 = 0.11 a.u., c_2 = 0.89 a.u., and $K_{0.5}$ = 34 mM; and for KdpD^1: c_1 = 0.33 a.u., c_2 = 0.67 a.u., and $K_{0.5}$ = 32 mM. Confidence regions were estimated by randomly sampling parameter space and including or excluding parameter sets according to F test relative to the best-fit parameters.

Mathematical Model

Details of the mathematical model and simulations are provided in the Supplemental Experimental Procedures.

SUPPLEMENTAL INFORMATION

Supplemental Information includes Supplemental Experimental Procedures, six figures, and three tables and can be found with this article online at http://dx.doi.org/10.1016/j.celrep.2016.05.081.

AUTHOR CONTRIBUTIONS

H.S., R.H., and K.J. designed the experiments. H.S. performed the experiments. F.T. and U.G. developed the mathematical model and F.T. performed simulations. H.S., F.T., R.H., U.G., and K.J. wrote the manuscript.

ACKNOWLEDGMENTS

This work was supported by the Deutsche Forschungsgemeinschaft: Center for integrated Protein Science Munich (CiPSM) (Exc114/2) and (JU270/15-1) (to K.J.) and Nanosystems Initiative Munich (NIM) (Exc4/2) and (GE1098/6-1) (to U.G.). F.T. was supported by a research fellowship of the Alexander von Humboldt Foundation. We thank Daniel Wilson (Gene Center Munich) and Erwin Frey (LMU Munich) for critically reading the manuscript and Andy Fohrmann for constructing plasmids encoding truncated KdpD variants (pPV5-3/ΔTM1-4, pBD/ΔTM1-4/10Gly, and pBD/ΔTM1-4/5[Gly,Ala]).

Received: February 29, 2016
Revised: April 15, 2016
Accepted: May 19, 2016
Published: June 16, 2016

REFERENCES

Altendorf, K., Siebers, A., and Epstein, W. (1992). The KDP ATPase of *Escherichia coli*. Ann. N Y Acad. Sci. *671*, 228–243.

Batchelor, E., and Goulian, M. (2003). Robustness and the cycle of phosphorylation and dephosphorylation in a two-component regulatory system. Proc. Natl. Acad. Sci. USA *100*, 691–696.

Bhate, M.P., Molnar, K.S., Goulian, M., and DeGrado, W.F. (2015). Signal transduction in histidine kinases: insights from new structures. Structure *23*, 981–994.

Booth, I.R. (1985). Regulation of cytoplasmic pH in bacteria. Microbiol. Rev. *49*, 359–378.

Bossemeyer, D., Borchard, A., Dosch, D.C., Helmer, G.C., Epstein, W., Booth, I.R., and Bakker, E.P. (1989). K^+-transport protein TrkA of *Escherichia coli* is a peripheral membrane protein that requires other *trk* gene products for attachment to the cytoplasmic membrane. J. Biol. Chem. *264*, 16403–16410.

Brandon, L., Dorus, S., Epstein, W., Altendorf, K., and Jung, K. (2000). Modulation of KdpD phosphatase implicated in the physiological expression of the kdp ATPase of *Escherichia coli*. Mol. Microbiol. *38*, 1086–1092.

Buurman, E.T., McLaggan, D., Naprstek, J., and Epstein, W. (2004). Multiple paths for nonphysiological transport of K^+ in *Escherichia coli*. J. Bacteriol. *186*, 4238–4245.

Cann, M. (2007a). A subset of GAF domains are evolutionarily conserved sodium sensors. Mol. Microbiol. *64*, 461–472.

Cann, M.J. (2007b). Sodium regulation of GAF domain function. Biochem. Soc. Trans. *35*, 1032–1034.

Cromie, M.J., Shi, Y., Latifi, T., and Groisman, E.A. (2006). An RNA sensor for intracellular Mg^{2+}. Cell *125*, 71–84.

Damnjanovic, B., and Apell, H.-J. (2014). KdpFABC reconstituted in *Escherichia coli* lipid vesicles: substrate dependence of the transport rate. Biochemistry *53*, 5674–5682.

Epstein, W. (2003). The roles and regulation of potassium in bacteria. Prog. Nucleic Acid Res. Mol. Biol. *75*, 293–320.

Epstein, W., and Kim, B.S. (1971). Potassium transport loci in *Escherichia coli* K-12. J. Bacteriol. *108*, 639–644.

Ferris, H.U., Dunin-Horkawicz, S., Hornig, N., Hulko, M., Martin, J., Schultz, J.E., Zeth, K., Lupas, A.N., and Coles, M. (2012). Mechanism of regulation of receptor histidine kinases. Structure *20*, 56–66.

García Véscovi, E., Soncini, F.C., and Groisman, E.A. (1996). Mg^{2+} as an extracellular signal: environmental regulation of *Salmonella* virulence. Cell *84*, 165–174.

Goujon, M., McWilliam, H., Li, W., Valentin, F., Squizzato, S., Paern, J., and Lopez, R. (2010). A new bioinformatics analysis tools framework at EMBL-EBI. Nucleic Acids Res. *38* (*Suppl*), W695–W699.

Heermann, R., and Jung, K. (2012). K^+ supply, osmotic stress and the KdpD/KdpE two-component system. In Two-component systems in bacteria, R. Gross and D. Beier, eds. (Norwich, UK: Caister Academic Press), pp. 181–198.

Heermann, R., Weber, A., Mayer, B., Ott, M., Hauser, E., Gabriel, G., Pirch, T., and Jung, K. (2009). The universal stress protein UspC scaffolds the KdpD/KdpE signaling cascade of *Escherichia coli* under salt stress. J. Mol. Biol. *386*, 134–148.

Heermann, R., Zigann, K., Gayer, S., Rodriguez-Fernandez, M., Banga, J.R., Kremling, A., and Jung, K. (2014). Dynamics of an interactive network composed of a bacterial two-component system, a transporter and K^+ as mediator. PLoS ONE *9*, e89671.

Heikaus, C.C., Pandit, J., and Klevit, R.E. (2009). Cyclic nucleotide binding GAF domains from phosphodiesterases: structural and mechanistic insights. Structure *17*, 1551–1557.

Huynh, T.N., and Stewart, V. (2011). Negative control in two-component signal transduction by transmitter phosphatase activity. Mol. Microbiol. *82*, 275–286.

Jung, K., and Altendorf, K. (1998). Individual substitutions of clustered arginine residues of the sensor kinase KdpD of *Escherichia coli* modulate the ratio of kinase to phosphatase activity. J. Biol. Chem. *273*, 26415–26420.

Jung, K., Tjaden, B., and Altendorf, K. (1997). Purification, reconstitution, and characterization of KdpD, the turgor sensor of *Escherichia coli*. J. Biol. Chem. *272*, 10847–10852.

Jung, K., Krabusch, M., and Altendorf, K. (2001). Cs^+ induces the *kdp* operon of *Escherichia coli* by lowering the intracellular K^+ concentration. J. Bacteriol. *183*, 3800–3803.

Kilian, C.T. (2005). Modern Control Technology (Delmar Thomson Learning).

Laermann, V., Ćudić, E., Kipschull, K., Zimmann, P., and Altendorf, K. (2013). The sensor kinase KdpD of *Escherichia coli* senses external K^+. Mol. Microbiol. *88*, 1194–1204.

Lüttmann, D., Heermann, R., Zimmer, B., Hillmann, A., Rampp, I.S., Jung, K., and Görke, B. (2009). Stimulation of the potassium sensor KdpD kinase activity by interaction with the phosphotransferase protein IIA(Ntr) in *Escherichia coli*. Mol. Microbiol. *72*, 978–994.

Marina, A., Waldburger, C.D., and Hendrickson, W.A. (2005). Structure of the entire cytoplasmic portion of a sensor histidine-kinase protein. EMBO J. *24*, 4247–4259.

Mével-Ninio, M., and Yamamoto, T. (1974). Conversion of active transport vesicles of *Escherichia coli* into oxidative phosphorylation vesicles. Biochim. Biophys. Acta *357*, 63–66.

Miller, J.H. (1992). A short course in bacterial genetics: a laboratory manual and handbook for *Escherichia coli* and related bacteria (Plainview, N.Y.: Cold Spring Harbor Laboratory Press).

Nissen, P., Hansen, J., Ban, N., Moore, P.B., and Steitz, T.A. (2000). The structural basis of ribosome activity in peptide bond synthesis. Science *289*, 920–930.

Roe, A.J., McLaggan, D., O'Byrne, C.P., and Booth, I.R. (2000). Rapid inactivation of the *Escherichia coli* Kdp K^+ uptake system by high potassium concentrations. Mol. Microbiol. *35*, 1235–1243.

Rothenbücher, M.C., Facey, S.J., Kiefer, D., Kossmann, M., and Kuhn, A. (2006). The cytoplasmic C-terminal domain of the *Escherichia coli* KdpD protein functions as a K^+ sensor. J. Bacteriol. *188*, 1950–1958.

Shinar, G., Milo, R., Martínez, M.R., and Alon, U. (2007). Input output robustness in simple bacterial signaling systems. Proc. Natl. Acad. Sci. USA *104*, 19931–19935.

Willett, J.W., and Kirby, J.R. (2012). Genetic and biochemical dissection of a HisKA domain identifies residues required exclusively for kinase and phosphatase activities. PLoS Genet. *8*, e1003084.

Zeng, Y., Han, X., and Gross, R.W. (1998). Phospholipid subclass specific alterations in the passive ion permeability of membrane bilayers: separation of enthalpic and entropic contributions to transbilayer ion flux. Biochemistry *37*, 2346–2355.

Cell Reports, Volume *16*

Supplemental Information

A Dual-Sensing Receptor Confers Robust Cellular Homeostasis

Hannah Schramke, Filipe Tostevin, Ralf Heermann, Ulrich Gerland, and Kirsten Jung

Supplemental Figures

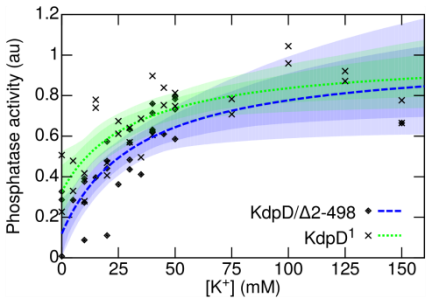

Figure S1: *In vitro* phosphatase activity of KdpD[1]. Related to Figs. 1, 2 and 4.
Full lines show the best-fit Michaelis form; shading denotes regions that contain all activity curves within 68% and 95% confidence regions. Data for KdpD/Δ2-498 is the same as in Fig. 1D.

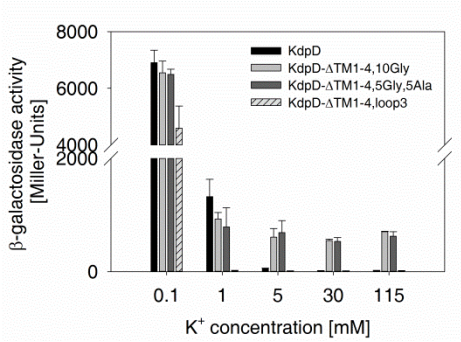

Figure S2: β-galactosidase activities of the reporter strain (*P*$_{kdpFABC}$*::lacZ*) carrying plasmids encoding KdpD and truncated KdpD variants. Related to Fig. 3. The truncated KdpD variants lack the four transmembrane domains and are linked by a 10 glycine (KdpD-ΔTM1-4,10Gly), 5 glycine 5 alanine (KdpD-ΔTM1-4,5Gly,5Ala) and the periplasmic loop sequence (KdpD-ΔTM1-4,loop3), respectively. β-galactosidase activity was determined after cultivation of cells in minimal medium at the indicated K^+-concentrations.

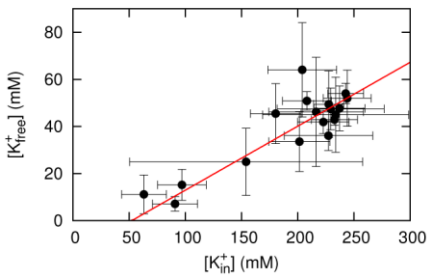

Figure S3: Intracellular free K^+. Related to Fig. 5.
Wild-type cells were grown in in minimal medium containing 10 mM K^+ and then shifted to minimal medium containing different K^+ concentrations. After 2 hours samples were taken and the intracellular K^+ concentration was determined. Measured intracellular free K^+ is plotted against total intracellular K^+. The full line shows the best linear fit, $[K^+_{free}]=0.27[K^+_{in}]-14$ mM.

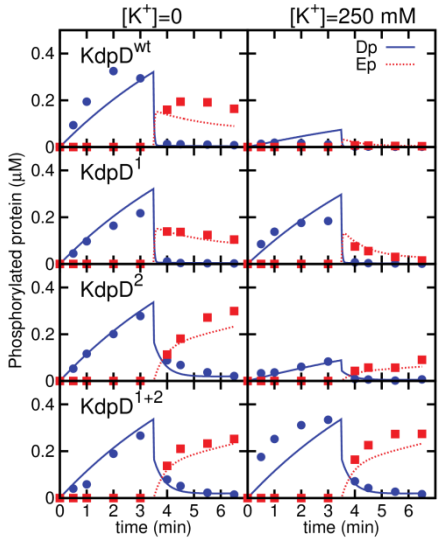

Figure S4: Fitting of *in vitro* model to experimental data. Related to Figs. 4 and 5.
Comparison of the dynamics of the mathematical model (lines) with experimental data (points) for all experimental conditions and strains.

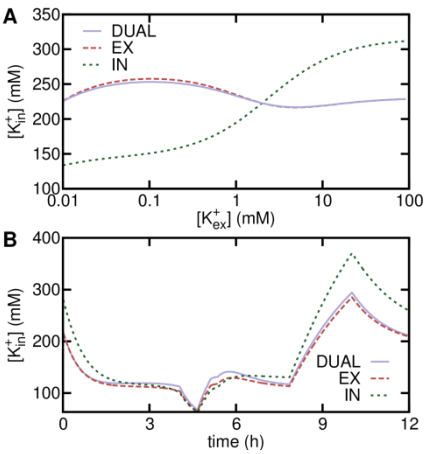

Figure S5: Intracellular K^+ for different regulation strategies. Related to Fig. 6.
(A) Steady-state intracellular K^+ concentration as a function of extracellular K^+ for different KdpD regulation strategies. (B) An example of the dynamic response of intracellular K^+ in a random environment.

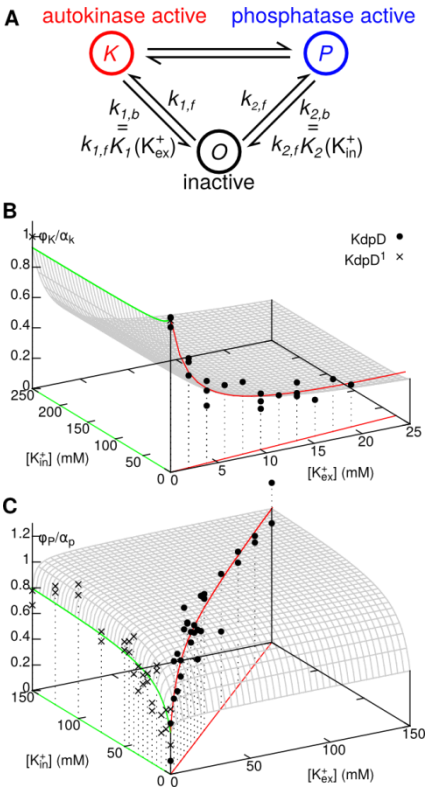

Figure S6: Fitting of KdpD state-switching model. Related to Fig. 5.
(A) KdpD switching model, showing the definition of the equilibrium constants K_1 and K_2. Parameters of the KdpD state-switching were determined by fitting to the autokinase (B) and phosphatase (C) activities measured *in vitro* for KdpD and KdpD^1 (data points), which lie along lines in the two-dimensional input space. The resulting parameters define an activity response surface as a function of internal and external K^+.

Supplemental Tables

Table S1: Strains used in this study (Related to Materials and Methods and SI Materials and Methods)

Strain	Feature / Construction comments	Source
DH5α	F^- Φ80*lacZ*ΔM15 Δ(*lacZYA-arg*F) U169 *recA1 endA1 hsdR17* (r_K^-, m_K^+) *phoA supE44* λ^- *thi*-1 *gyrA96 relA1*	Promega
MG1655	*E. coli* K-12 reference strain	(Blattner *et al.*, 1997)
BL21 (DE3/pLysS)	F^- *ompT hsdSB* ($r_B^- m_B^-$) *dcm gal* (DE3) pLysS (Cm^R)	(Studier & Moffatt, 1986)
TKR2000	Δ*kdpFABCDE trkA405 trkD1 atp706*	(Kollmann & Altendorf, 1993)
HAK006	CSH26 *ΔkdpABCD::neo λattB::kdpFA'-lacZ* Δ*(lac-pro)ara thi*	(Nakashima *et al.*, 1993)
LF3	MG1655 *rpsL150* P_{kdp}*::lacZ;*Kan^s $Strp^r$	(Fried *et al.*, 2012)
HS1	MG1655 *rpsL150* P_{kdp}*::lacZ; kdpD::rpsL-neo*, Kan^r Str^s	this study
HS2	MG1655 *rpsL150* P_{kdp}*::lacZ;* $kdpD^{Pro466Ala,Thr469Ala,Leu470Ala,Val472Ala}$, Kan^s Str^r	this study
HS3	MG1655 *rpsL150* P_{kdp}*::lacZ;* $kdpD^{Thr677Ala}$, Kan^s Str^r	this study
HS4	MG1655 *rpsL150* P_{kdp}*::lacZ;* $kdpD^{Pro466Ala,Thr469Ala,Leu470Ala,Val472Ala,Thr677Ala}$, Kan^s Str^r	this study

Table S2: Primers used in this study (Related to Materials and Methods and SI Materials and Methods)

	Name	Sequence	Restriction site	Reference
Native				
P1	NotI_s	GTG GTT GCG GCC GCG TTA TGC GCC	*NotI*	this study
P2	HindIII_as	AAA ACA GCC AAG CTT TGT CAC ATA TC	*HindIII*	this study
P3	Kdp730_as	CCA CTC TTT CTT CAA ATT AAA GCC GCC		this study
Artificial modification of amino acids				
P4	F463A_s	CGA TCT CTT TGC TAT CGC CCC ACG C		this study
P5	F463A_as	GCG TGG GGC GAT AGC AAA GAG ATC G		this study
P6	I464A_s	CGA TCT CTT TTT TGC CGC CCC ACG C		this study
P7	I464A_as	GCG TGG GGC GGC AAA AAA GAG ATC G		this study
P8	P466A_s	TTT ATC GCC GCA CGC GGT ACC		this study
P9	P466A_as	GGT ACC GCG TGC GGC GAT AAA		this study
P10	R467A_s	ATC GCC CCA GCC GGT ACC CTC GCC GTC		this study
P11	R467A_as	GAC GGC GAG GGT ACC GGC TGG GGC GAT		this study
P12	T469A_s	CGG TGC CCT CGC CGT CTC TGA TG		this study
P13	T469A_as	CAT CAG AGA CGG CGA GGG CAC CG		this study
P14	L470A_s	CGG TAC CGC CGC CGT CTC TGA TG		this study
P15	L470A_as	CAT CAG AGA CGG CGG CGG TAC CG		this study
P16	V472A_s	CGG TAC CCT CGC CGC CTC TGA TG		this study
P17	V472A_as	CAT CAG AGG CGG CGA GGG TAC CG		this study
P18	S473A_s	CTC GCC GTC GCT GAT GTG CAA TAT C		this study

P19	S473A_as	GAT ATT GCA CAT CAG CGA CGG CGA G		this study
P20	T677A_s	ATG ATT TAC GCG CGC CGC TTA CG		this study
P21	T677A_as	CGT AAG CGG CGC GCG TAA ATC AT		this study
P22	P466A,V472A, L470A_s	TTA TCG CCG CAC GCG GTA CCG CAG CCG CAT CTG ATG		this study
P23	P466A, V472A, L470A_as	CAT CAG ATG CGG CTG CGG TAC CGC GTG CGG CGA TAA		this study
P24	P466A, T469A,V472A, L470A_s	GCA CGC GGT GCC GCA GCC GCA TC		this study
P25	P466A, T469A,V472A, L470A_as	GAT GCG GCT GCG GCA CCG CGT GC		this study
Chromosomal insertion of point mutations via pRED®/ET® counter selection				
P26	KdpD_up	GTG GCG CTA TTT TAT GGA CGC TGG CCT TCA GTG GTT GCC ACC GTC ATT AAG GCC TGG TGA TGA TGG CGG GAT CG		this study
P27	KdpD_low	GGG CGT GGG GTG ATC CTT CGC TTG CCA GAT CGA GCG TTA AGA TTT CTG CCT CAG AAG AAC TCG TCA AGA AGG CG		this study
Generation of truncated *kdpD* variants				
P28	499_NdeI_s	GGC GCA TAT GCG TTA TCA GGC GCG G	*NdeI*	this study
P29	499+505_BamHI_as	AGC TCG GAT CCT CAC ATA TCC TCA TG	*BamHI*	this study
P30	TM1-4_sense	GTA CAA ATT CAG CGT TAT CAG GCG CGA GTA GCC CGT TAC CGC		this study
P31	TM1-4_antisense	CGC CTG ATA ACG CTG AAT TTG TAC ACG CCA CTT GTC TTT AAA		this study
P32	SpeI_sense	CTC GAT CAG GTA CTA GTC GCG CGC CTT		this study
P33	MluI_antisense	TTC ATA TAA GTG ACG CGT GCG TTG C		this study
P34	Deca-Gly sense	CGG CGG CGG CGG CGG CGG CGG CGG CGG CGG CA		this study
P35	Deca-Gly antisense	CAT GGC CGC CGC CGC CGC CGC CGC CGC CGC CGT CTA G		this study
P36	Deca-Gly,Ala sense	CGG TGC TGG TGC TGG TGC TGG TGC TGG TGC TA		this study
P37	Deca Gly,Ala antisense	CAT GGC CAC GAC CAC GAC CAC GAC CAC GAC CAC GAT CTA G		this study
P38	delta TM4_s	CCT CGC CGT CTC TTA TCA GGC GCG G		this study
P39	delta TM4_as	CCG CGC CTG ATA AGA GAC GGC GAG G		this study
P40	delta TM1-3_s	GAT AAC CGC TCT TTT ATC GCC CCA C		this study
P41	delta TM1-3_as	GTG GGG CGA TAA AAG AGC GGT TAT C		this study
	XmaI_s	ACC CGG GGA TCC GTC GAC CTG CAG GTC		this study

Table S3: Plasmids used in this study (Related to Materials and Methods and SI Materials and Methods)

Plasmid	**Feature / Construction comments**	**Source**
General plasmids		

pET16B	Amp^r-cassette, T7-promoter, pBR322 origin, 5‘-His-tag coding sequence, *lacI*-coding sequence, *lac* operator	Novagen (Merck Millipore)
pRED/ET	λ-RED recombinase in pBAD24, Amp^r	Gene Bridges
pBAD18	Amp^r-cassette, pBR322 origin	(Guzman *et al.*, 1995)
pBD	*kdpD* in pBAD18, Amp^r	(Jung *et al.*, 1998)
pPV5-3	*kdpD*6His in pKK223-3	(Jung & Altendorf, 1998)
pEE	10His-*kdpE* under PT7-control in pET16B, Amp^r	(Heermann *et al.*, 2003)
Truncated *kdpD* variants		
pBD/6-92	*kdpD*$^{\Delta 12\text{-}395}$ in pBAD18	(Jung & Altendorf, 1998b)
pET16b/C3	*kdpD*$^{\Delta 2\text{-}498}$ in pET/16b	this study
pPV5-3/ΔTM1-4	*kdpD*$^{\Delta G401\text{-}V498}$ in pPV/5-3	this study
pBD/ΔTM1-4/10Gly	*kdpD*$^{\Delta G401\text{-}V498/V397G,Q501R,A502S/\Delta I399\text{-}Y400,R499\text{-}Y500,10Gly}$ in pBAD18	this study
pBD/ΔTM1-4/5(Gly,Ala)	*kdpD*$^{\Delta G401\text{-}V498/V397G,Q501R,A502S/\Delta I399\text{-}Y400,R499\text{-}Y500\ 5(Gly,Ala)}$ in pBAD18	this study
pBD/ΔTM1-4/loop3	*kdpD*$^{\Delta F391\text{-}F462,\ \Delta D474\text{-}R500)}$ in pBAD18	this study
Artificial modification of amino acids Phe463-Ser473		
pBD/F463A	*kdpD*^{Phe463Ala} in pBD	this study
pBD/I464A	*kdpD*^{Ile464Ala} in pBD	this study
pBD/P466A	*kdpD*^{Pro466Ala} in pBD	this study
pBD/R467A	*kdpD*^{Arg467Ala} in pBD	this study
pBD/T469A	*kdpD*^{Thr469Ala} in pBD	this study
pBD/L470A	*kdpD*^{Leu470Ala} in pBD	this study
pBD/V472A	*kdpD*^{Val472Ala} in pBD	this study
pBD/S473A	*kdpD*^{Ser473Ala} in pBD	this study
pBD/#3	*kdpD*$^{Pro466Ala,\ Thr469Ala,\ L470Ala,\ V472Ala}$ in pBD	this study
Artificial inactivation of the phosphatase activity		
pBD/T677A	*kdpD*^{Thr677Ala} in pBD	this study
pBD/#4	*kdpD*$^{Pro466Ala,\ Thr469Ala,\ Leu470Ala,\ Val472Ala,\ Thr677Ala}$ in pBD	this study

Supplemental Experimental Procedures

Materials

Ni^{2+}-NTA resin and the Penta-His antibody were obtained from Qiagen (Hilden, Germany). NAP-5 columns and [γ-^{32}P]ATP were purchased from GE Healthcare (Freiburg, Germany) and Perkin Elmer (Groningen, Netherlands), respectively. Goat anti-(rabbit IgG)-alkaline phosphatase was obtained from Biomol (Hamburg, Germany), and silicone oil (DC550) was from Serva (Heidelberg, Germany). All other reagents were reagent grade and obtained from commercial sources.

Bacterial strains, oligonucleotides and plasmids

Genotypes of strains and plasmids used in this study are listed in Table S1 and S3. Primer sequences are listed in Table S2. *E. coli* strain MG1655 (wild type K-12 strain) was used for studies of intracellular K^+ concentrations. *E. coli* strain HAK006 was used for reporter assays with plasmid encoded *kdpD* (Nakashima *et al.*, 1993). For protein overproduction of soluble proteins *E. coli* BL21 (DE3/pLysS) and for preparation of membrane vesicles *E. coli* TKR2000 was used. Strains carrying chromosomal point mutations within *kdpD* (HS2, HS3 and HS4) are based on the reporter strain LF3 and were generated by using Red®/ET® recombination technology in combination with *rpsL* counter-selection (Heermann *et al.*, 2008). The linear DNA fragments for homologous recombination carrying corresponding point mutations were amplified from plasmids pBD/#3, pBD/T677A and pBD/#4 (see Table S3), respectively by using primers NotI_s and Kdp730_as (see Table S2). All point mutations were introduced in pBD via overlap PCR using the primers NotI_s, HindIII_as and the corresponding primers containing point mutations (Table S2). The products were ligated into pBD using NotI and HindIII restriction enzymes. The truncated variant *kdpD/Δ2-498* was generated with the listed primers and cloned into pET16b using NdeI and BamHI restriction sites. Plasmid pPV5-3/ΔTM1-4 was generated by overlap PCR using primer pairs TM1-4_sense + MluI_antisense and SpeI_sense + TM1-4_antisense and subsequent ligation in pPV5-3 using MluI and SpeI restriction sites. The 10 Gly and 5(Gly,Ala) linkers were inserted via BglII and KpnI restriction sites in pPV5-3/ΔTM1-4 by using the annealed oligonucleotides Deca-Gly sense + Deca-Gly antisense and Deca-Gly,Ala sense + Deca-Gly,Ala antisense. Afterwards truncated *kdpD* variants were cloned in pBAD18 using XmaI and HindIII restriction sites resulting in plasmids pBD/ΔTM1-4/10Gly and pBD/ΔTM1-4/5(Gly,Ala). Plasmid pBD/ΔTM1-4/loop3 was created in two steps. In the first step nucleotides encoding amino acids of TM4 were removed by a two-step overlap PCR using primer pairs XmaI_s + delta TM4_as and delta TM4_s + HindII_as and subsequent cloning in pBD using SpeI and HindII restriction sites. The resulting plasmid was used as template for the second step, in which nucleotides encoding amino acids of TM1-3 were removed by another two-step overlap PCR using primer pairs XmaI_s + delta TM1-3_as and delta TM1-3_s + HindIII_as. Subsequent cloning in pBD using SpeI and HindIII restriction sites resulted in plasmid pBD/ΔTM1-4/loop3.

Cell fractionation and preparation of membrane vesicles

E. coli strain TKR2000 transformed with plasmids pBD or its derivatives was grown aerobically at 37°C in KML complex medium (1% (w/v) tryptone, 0.5% (w/v) yeast extract, and 1% (w/v) KCl) supplemented with ampicillin (100 µg/ml). Cells were induced at OD_{600}=0.5 with 0.2% (w/v) arabinose and grown for another three hours. After harvesting, the cells were washed with buffer (50 mM Tris/HCl pH 7.5, 10 mM $MgCl_2$) and disrupted by passage through a Cell disruptor (Constant Cell Disruption Systems, Northants, UK) at 1.35 kbar and 4°C in disruption buffer [50 mM Tris/HCl pH 7.5, 10% (v/v) glycerol, 10 mM $MgCl_2$, 1 mM dithiotreitol, 0.5 mM phenylmethylsulfonylfluoride, and 0.03 mg/ml DNase]. After removal of intact cells and cell debris by centrifugation (9.000 × g, 10 min), membrane vesicles were collected by centrifugation at 160.000 × g for 60 min. Membrane vesicles were washed with low ionic strength buffer (10 mM Tris/HCl, pH 7.5, 3 mM EDTA), centrifuged again and resuspended in 50 mM Tris/HCl, pH 7.5 containing 10% (v/v) glycerol. Vesicles were frozen in liquid nitrogen and stored at -80°C until use.

Overproduction and purification of soluble proteins

E. coli strain BL21 transformed with plasmids pET16b/C3 and pEE, respectively, was grown aerobically at 37°C in LB complex medium [1% (w/v) tryptone, 0.5% (w/v) yeast extract, and 1% (w/v) NaCl] supplemented with ampicillin (100 µg/ml). Gene expression was induced at OD_{600}=0.5 with 0.5 mM IPTG and cells were grown for another three hours. After harvesting the cells were washed with buffer (50 mM Tris/HCl pH 7.5, 10 mM $MgCl_2$) and disrupted by passage through a Cell disruptor (Constant Cell Disruption Systems, Northants, UK) at 1.35 kbar and 4°C in disruption buffer [50 mM Tris/HCl pH 7.5, 10% (v/v) glycerol, 10 mM $MgCl_2$, 1 mM dithiotreitol, 0.5 mM phenylmethylsulfonylfluoride, and 0.03 mg/ml (w/v) DNase]. After removal of intact cells and cell debris by centrifugation (9.000 × g, 10 min), the cytosol was frozen at -80°C. Purification was performed as described before

(Heermann *et al.*, 2003). Deviating from this purification protocol, KdpD/Δ2-498 (pET16b/C3) was eluted with 250 mM imidazole

Mathematical model – KdpD switching dynamics

We model the enzymatic activities of KdpD by assuming that the protein has three conformational states, which we label as *K*, *P* and *O*. The occupancy of these states across the population of KdpD molecules is assumed to be in a dynamic equilibrium (see Fig. S6A). The autokinase activity is taken to be proportional to the probability of the system to be in the *K* state, while the phosphatase activity is proportional to the probability of being in the *P* state. The occupancies are given, in terms of the equilibrium constants of the transitions to and from the catalytically inactive *O* state, by $\varphi_{\mathrm{K}} = \frac{K_2}{K_1+K_2+K_1K_2}$, $\varphi_{\mathrm{P}} = \frac{K_1}{K_1+K_2+K_1K_2}$. Considering the requirement for external K^+-sensing for autokinase activity regulation, and that phosphatase regulation does not require external K^+ sensing, we took the equilibrium constants to depend on different K^+ pools according to $K_1([\mathrm{K}^+_{\mathrm{ex}}]) = \frac{a_k+b_k[\mathrm{K}^+_{\mathrm{ex}}]}{c_k+[\mathrm{K}^+_{\mathrm{ex}}]}$, $K_2([\mathrm{K}^+_{\mathrm{in}}]) = \frac{a_p+b_p[\mathrm{K}^+_{\mathrm{in}}]}{c_p+[\mathrm{K}^+_{\mathrm{in}}]}$.

We sought to estimate the parameters appearing in these equilibrium constants using the *in vitro* measured activity data. Substituting the above expressions for K_1 and K_2 into φ_{K} and φ_{P}, the result is a two-dimensional regulation function for each enzymatic activity. However, out *in vitro* activity measurements do not span this input space, as it is not possible to selectively apply different K^+ concentrations to the extracellular and intracellular portions of the protein. The *in vitro* activity measurements for wild-type KdpD provide us with the values of the enzymatic activities only along one lines in input space, namely $[\mathrm{K}^+_{\mathrm{ex}}] = [\mathrm{K}^+_{\mathrm{in}}]$. However, we reasoned that the activity of the KdpD[1] variant that is insensitive to extracellular K^+, is equivalent to the enzymatic activities along the line $[\mathrm{K}^+_{\mathrm{ex}}] = 0$ (see Fig. S6).

We therefore estimated the values of the parameters that best reproduced the activity regulation *in vitro* by simultaneous least-squares fitting to the autokinase and phosphatase data from wild-type KdpD and KdpD[1] (Fig. 1C&D and S1). Since the enzymatic activity measurements cannot identify the actual occupancy of each state, but only relative changes in occupancy, we introduced additional weighting factors α_k and α_p to account for the scaling of occupancy to activity. Ultimately, therefore, we used the Levenberg-Marquardt method to estimate the parameters that minimize the function

$$\sum_{i\in\text{data points}}\left[\frac{\varphi_{\mathrm{K}}([\mathrm{K}^+_i],[\mathrm{K}^+_i])}{\alpha_k} - k_i^{\mathrm{WT}}\right]^2 + \sum_{i\in\text{data points}}\left[\frac{\varphi_{\mathrm{P}}([\mathrm{K}^+_i],[\mathrm{K}^+_i])}{\alpha_p} - p_i^{\mathrm{WT}}\right]^2 + \sum_{i\in\text{data points}}\left[\frac{\varphi_{\mathrm{K}}(0,[\mathrm{K}^+_i])}{\alpha_k} - k_i^{1}\right]^2 + \sum_{i\in\text{data points}}\left[\frac{\varphi_{\mathrm{P}}(0,[\mathrm{K}^+_i])}{\alpha_p} - p_i^{1}\right]^2,$$

where k_i and p_i are the individual autokinase and phosphatase activity measurements, and the superscript denotes either wild-type or the KdpD[1] variant. The resulting best-fit parameter values (Fig. S6) were a_k=18.4 mM, b_k=11.7, c_k=9.09 mM, α_k=0.31, a_p=59.3 mM, b_p=4.35, c_p=4.76 mM, α_p=0.16.

Mathematical model - *in vitro*. We next sought a model of KdpD/KdpE phosphorylation that was consistent with the dynamics measured *in vitro* for all KdpD variants. The proposed phosphorylation and phosphotransfer reactions were incorporated into a pair of differential equations describing how the concentration of phosphorylated KdpD (Dp) and phosphorylated KdpE (Ep) changes over time:

$$\frac{d\mathrm{Dp}}{dt} = \frac{\kappa_{\mathrm{auto}}}{v}\left[\varphi_{\mathrm{K}}\big((1-\delta_1)[\mathrm{K}^+],[\mathrm{K}^+]\big)(\mathrm{Dtot}-\mathrm{Dp}) - K_{\mathrm{auto}}\mathrm{Dp}\right] - \frac{\kappa_{\mathrm{trans}}}{1+\delta_2\gamma}\left[\mathrm{Dp}(\mathrm{Etot}-\mathrm{Ep}) - K_{\mathrm{trans}}(\mathrm{Dtot}-\mathrm{Dp})\mathrm{Ep}\right], \quad (1)$$

$$\frac{d\mathrm{Ep}}{dt} = \frac{\kappa_{\mathrm{trans}}}{1+\delta_2\gamma}\left[\mathrm{Dp}(\mathrm{Etot}-\mathrm{Ep}) - K_{\mathrm{trans}}(\mathrm{Dtot}-\mathrm{Dp})\mathrm{Ep}\right] - \kappa_{\mathrm{p}}\varphi_{\mathrm{P}}((1-\delta_1)[\mathrm{K}^+],[\mathrm{K}^+])(\mathrm{Dtot}-\mathrm{Dp})\mathrm{Ep}. \quad (2)$$

Here Dtot and Etot denote the total concentrations of KdpD and KdpE in the system and v is the relative system volume. The first two reactions in Eq. 1 describe the reversible phosphorylation of KdpD. We assume that KdpD molecules in the *K* state undergo autophosphorylation with a rate that depends on the ATP concentration (see below). Phosphorylated KdpD cannot catalyze any reaction but phosphotransfer to KdpE. The last two terms in Eq. 1 and the corresponding complementary terms in Eq. 2 describe the reversible phosphotransfer between KdpD and KdpE. Phosphotransfer is assumed to occur at a constant rate, insensitive to K^+. Following phosphotransfer, unphosphorylated KdpD rapidly equilibrates between the three conformational states (Fig. 5A). Finally, the last term of Eq. 2 models dephosphorylation of phospho-KdpE by KdpD; we assume that only unphosphorylated KdpD

acts as a phosphatase in this reaction. The influence of K^+ on the enzymatic activity is introduced via the occupancy functions φ_K and φ_P, described above. Since in our *in vitro* assay both the periplasmic and cytoplasmic sides of the KdpD protein are exposed to the same medium, we use the same $[K^+]$ for both external and internal sensing. We simulated the KdpD^2 mutation in the state-switching model by assuming that the *P* conformation was inaccessible, and recalculating the occupancy of the *K* state according to $K_1([K^+_{ex}])$ only.

The indicator functions δ_i are used to denote variants of the KdpD protein, with δ_1=1 if KdpD carries the amino-acid substitutions of variant 1 (KdpD$_1$ or KdpD$_{1+2}$) and δ_1=0 otherwise (wild-type or KdpD$_2$), and similarly for variant 2. We found that removal of KdpD autokinase activity in the model was not sufficient to reproduce the experimental results for the KdpD^2 and KdpD^{1+2} variants, resulting in a faster decrease in the level of phospho-KdpD upon addition of KdpE than observed experimentally. Agreement with experiment was improved only if we allowed variation 2, in addition to eliminating KdpD phosphatase activity, to alter the rates of phosphotransfer between KdpD and KdpE compared to wild-type. This is incorporated via the parameter γ. Such an effect may arise, for example, because the variation also indirectly changes the KdpD-KdpE binding affinity. Initially we set Dp=Etot=Ep=0 μM, Dtot=2 μM and v=1 at time t=0. To model the later addition of KdpE we set Etot=8 μM at t=3.5 min. The addition of KdpE also doubles the volume of the system; therefore at this time we also halve the concentrations $[K^+]$, Dtot and Dp and set v=2. The inclusion of the factor v^{-1} in the first term of Eq. 1 models the slowing down of KdpD (de-)phosphorylation due to the dilution of ATP and ADP in the medium.

The values of the kinetic rate parameters κ_{auto}, κ_{trans} and κ_{p}, equilibrium constants K_{auto} and K_{trans}, and variant effect γ, were determined by Monte Carlo fitting to the experimental data. Initial trial parameter values were chosen from a log-normal distribution with median 1 and scale parameter σ=5. The trajectory of the system was evaluated for these parameters, and the total squared deviation from the experimental time-course data weighted by the data value, $Z^2 = \sum_{i\in\text{data points}} \frac{(x(i)_{\text{experiment}} - x(i)_{\text{model}})^2}{x(i)_{\text{experiment}}}$, was determined. The value of one randomly chosen parameter was then multiplied by a factor e^{ξ} with ξ chosen from a Gaussian distribution with zero mean and standard deviation 0.1. The trajectories and deviation Z were then re-evaluated for the new parameter set. If the new parameters did not provide an improved fit (i.e. if they resulted in a larger Z), then the parameters were reverted to their previous value and a new random modification was made; otherwise, the current parameters were retained and modified in the next round. This procedure was repeated for a total of 10^6 iterations. We found that a small fraction of optimization runs (~5%) became trapped in poorly-fitting regions of parameter space, while the majority of realizations converged to a single consensus parameter set (κ_{auto}=0.19 min^{-1}, K_{auto}=0.47, κ_{trans}=4.3 μM^{-1} min^{-1}, K_{trans}=0.25, γ=14 and κ_{p}=8.9 μM^{-1} min^{-1}) when initialized with a range of initial parameter combinations.

Mathematical model – *in vivo* model and parameter fitting. In our *in vivo* model we use the same reactions scheme as above to describe the dynamics of KdpD/KdpE phosphorylation. However, we must now introduce the different pools of extracellular and intracellular K^+. As most intracellular K^+ is bound to macromolecules, it is important to distinguish between bound and free ions when considering the effects of intracellular K^+. To this end we fit a linear relationship $[K^+_{\mathrm{free}}] = f_0 + f_{\mathrm{free}}[K^+_{\mathrm{in}}]$ to the experimentally-measured intracellular total and free K^+ concentrations using the Deming method with the residuals at each point weighted by the corresponding variance in the experimental measurements. The resulting best fit parameters were f_0=-14 mM and f_{free}=0.27 (Fig. S3). For any $[K^+_{\mathrm{in}}]$ that this relationship indicated a negative $[K^+_{\mathrm{free}}]$, $[K^+_{\mathrm{free}}]$ was set equal to zero. The KdpD/KdpE phosphotransfer reactions therefore became

$$\frac{d\mathrm{Dp}}{dt} = \kappa_{\mathrm{auto}}\left[\varphi_K\left((1-\delta_1)[K^+_{ex}],[K^+_{free}]\right)(\mathrm{Dtot}-\mathrm{Dp}) - K_{\mathrm{auto}}\mathrm{Dp}\right] - \frac{\kappa_{\mathrm{trans}}}{1+\delta_2\gamma}[\mathrm{Dp}(\mathrm{Etot}-\mathrm{Ep}) - K_{\mathrm{trans}}(\mathrm{Dtot}-\mathrm{Dp})\mathrm{Ep}], \quad (3)$$

$$\frac{d\mathrm{Ep}}{dt} = \frac{\kappa_{\mathrm{trans}}}{1+\delta_2\gamma}[\mathrm{Dp}(\mathrm{Etot}-\mathrm{Ep}) - K_{\mathrm{trans}}(\mathrm{Dtot}-\mathrm{Dp})\mathrm{Ep}] - \kappa_{\mathrm{p}}\varphi_P\left((1-\delta_1)[K^+_{ex}],[K^+_{free}]\right)(\mathrm{Dtot}-\mathrm{Dp})\mathrm{Ep}. \quad (4)$$

We assumed that the total concentration of KdpD and KdpE are constant, and set these values to Dtot=0.04 μM, Etot=0.08 μM (Surmann *et al.*, 2014). These equations were then supplemented by a model of KdpFABC production, K^+ import, and population growth.

As described in the Introduction, K^+ ions are imported into the cell by the high-affinity (HA) KdpFABC transporter and by constitutively produced low-affinity (LA) transporters. We described the rates of each of these reactions as a Michaelis-Menten function of the external K^+ concentration, $[K^+_{ex}]$, such that $[K^+_{in}]$ evolves according to

$$\frac{d[K^+_{in}]}{dt} = v_{\mathrm{LA}}\frac{[K^+_{ex}]}{[K^+_{ex}]+K_{\mathrm{m,LA}}} + v_{\mathrm{HA}}\mathrm{F}\frac{[K^+_{ex}]}{[K^+_{ex}]+K_{\mathrm{m,HA}}} - \mu[K^+_{in}], \quad (5)$$

where F is the concentration of KdpFABC transporters. The transporter affinities have been estimated previously and are set to $K_{\mathrm{m,LA}}$=2 mM and $K_{\mathrm{m,HA}}$=2 μM (Schlösser *et al.*, 1995, Rhoads *et al.*, 1976). We assumed that export of K^+ is negligible under our experimental conditions. The final term in Eq. 5 models dilution of K^+ by population growth with growth rate μ. The depletion of K^+ from the environment was described by the complement of the transport terms in Eq. 5, but scaled by the ratio of total cell volume to system volume, V(<<1),

$$\frac{d[\mathrm{K}^+_{\mathrm{ex}}]}{dt} = -\mathrm{V}\left[\upsilon_{\mathrm{LA}}\frac{[\mathrm{K}^+_{\mathrm{ex}}]}{[\mathrm{K}^+_{\mathrm{ex}}]+K_{\mathrm{m,LA}}} + \upsilon_{\mathrm{HA}}\mathrm{F}\frac{[\mathrm{K}^+_{\mathrm{ex}}]}{[\mathrm{K}^+_{\mathrm{ex}}]+K_{\mathrm{m,HA}}}\right]. \quad (6)$$

Next we considered the regulation of KdpFABC levels. Phospho-KdpE dimerizes and binds to the *kdpFABC* promoter, thereby activating the transcription of the *kdpFABC* operon encoding the high-affinity K^+ transporter complex (Nakashima *et al*., 1993). We assumed that both the dimerization of phospho-KdpE and the binding to DNA are fast, and thus we simply took the probability that the *kdpFABC* activator site is bound at any time to be given by

$$p(\mathrm{Ep}) = \frac{\mathrm{Ep}^2}{\mathrm{Ep}^2+K^2_{\mathrm{DNA}}}. \quad (7)$$

We took K_{DNA}=0.25 μM, in the range of previous measurements (Narayanan *et al.*, 2012). We then assumed that the concentration of KdpFABC transporters, F, evolves according to

$$\frac{d\mathrm{F}}{dt} = k_{\mathrm{tr}}\,p(\mathrm{Ep}) - \left[\mu + k_{\mathrm{deg}}(\mathrm{F})\right]\mathrm{F}. \quad (8)$$

For simplicity we did not model transcription and translation in detail, but rather assumed that KdpFABC is produced at an effective production rate k_{tr} when KdpE binds to the *kdpFABC* promoter. The second term in Eq. 8 accounts for both dilution due to growth, and potentially non-linear turnover of KdpFABC (Heermann *et al.*, 2014) with rate

$$k_{\mathrm{deg}}(\mathrm{F}) = k_{\mathrm{deg,0}} + k_{\mathrm{deg,F}}\mathrm{F}. \quad (9)$$

Finally, we accounted for the growth of the population over time. We assumed that the cell mass, or equivalently the volume fraction, increases according to

$$\frac{d\mathrm{V}}{dt} = \mu\mathrm{V}. \quad (10)$$

Since the detailed effects of changing intracellular K^+ concentration on population growth are not known, we used a phenomenological growth model wherein the growth rate depends on the intracellular K^+ concentration according to $\mu([\mathrm{K}^+_{\mathrm{in}}])=\mu_{\mathrm{max}}\frac{[\mathrm{K}^+_{\mathrm{in}}]^3}{[\mathrm{K}^+_{\mathrm{in}}]^3+K^3_{\mu}}$. This form together with the parameter values μ_{max}=0.011min^{-1} and K_{μ}=70 mM were chosen such that the resulting population dynamics match the experimentally measured growth curves when the simulated intracellular K^+ concentration also follows the corresponding experimentally observed values.

We once again sought parameter combinations that give the best fit to the experimental data. For this purpose we used the four data sets describing the *in vivo* response that are shown in Fig. 5: time-course measurements of (i) intracellular and (ii) extracellular K^+ concentrations and (iii) OD_{600}, for initial environmental K^+ concentrations of 10 mM, 1 mM and 0.1 mM; and (iv) KdpFABC protein copy numbers two hours after transfer to media with varying environmental K^+ levels. Since we would not expect the parameters for the KdpD/KdpE phosphorylation reactions *in vivo* to match with their *in vitro* values, these were initialized with their *in vitro* values but were subsequently allowed to vary. The additional parameters remaining to be determined that could not be estimated from previous measurements were: the transporter rates υ_{LA} and υ_{HA}; the maximal KdpFABC production rate k_{tr}; and the parameters of the KdpFABC degradation function, $k_{\mathrm{deg,0}}$ and $k_{\mathrm{deg,F}}$. A similar optimization procedure was employed as described above for the *in vivo* model. However, rather than the score function Z described above, we scaled the residual of the model from the data by the experimental uncertainty: $Z^2 = \sum_{i\in\text{data points}}\frac{(x(i)_{\mathrm{model}}-x(i)_{\mathrm{experiment}})^2}{\sigma(i)^2_{\mathrm{experiment}}}$, where $x(i)_{\mathrm{experiment}}$ and $\sigma(i)_{\mathrm{experiment}}$ are respectively the mean and standard deviation of the experimental data and the sum runs over all data sets described above.

All simulations of the *in vivo* model were initialized with Dp=Ep=0, $[\mathrm{K}^+_{\mathrm{in}}]$=250 mM, F=0, and V=2×10^{-4}. The value of the volume fraction V was subsequently scaled by a factor 1150 to match the scale of OD_{600} measurements. To mimic the preparation of cells in overnight culture with abundant K^+ we then evolved the model equations, but without depletion of extracellular K^+ or population growth (i.e. $\frac{d[\mathrm{K}^+_{\mathrm{ex}}]}{dt}=\frac{d\mathrm{V}}{dt}=0$), for 12 hours of simulated time in

an environment with constant extracellular concentration $[K^+_{ex}]$=10 mM. After this time, $[K^+_{ex}]$ was changed to the value of interest and the evolution of the extracellular concentration and population size were activated.

Multiple runs of the optimization procedure were again performed with different initial trial parameters. The best-fit set of parameters, used in Figs. 5 and 6, was as follows: κ_{auto}=0.76 min^{-1}, K_{auto}=0.18, κ_{trans}=1.1×10^4 μM^{-1}min^{-1}, K_{trans}=0.34, γ=0 and κ_{p}=32 μM^{-1} min^{-1}; υ_{LA}=2.3 mM min^{-1}, υ_{HA}=0.40 μM min^{-1}; k_{tr}=5400 min^{-1}, $k_{\mathrm{deg,0}}$=0.006 min^{-1} and $k_{\mathrm{deg,F}}$=4.4×10^{-7} min^{-1}. Of these parameters, those governing the rate of transport of K^+ were well constrained by the data, and produced consistent values across all realizations. Parameters describing *kdpFABC* expression and turnover were less restricted in their absolute values, although the ratios $k_{\mathrm{tr}}/k_{\mathrm{deg}}$ lay in narrow range. Among the parameters describing KdpD/KdpE phosphorylation, we found that the equilibrium constants K_{auto} and K_{trans} were precisely determined, as was γ. However, since the *in vitro* data provides no information about the phosphorylation dynamics per se, the kinetic rates of the various phosphorylation reactions were largely unconstrained by the data, and took a wide range of values in different realizations.

Alternate regulation strategies. To test different regulation strategies, we altered the model equations as follows. For the wild-type dual-sensing strategy (DUAL) we used the KdpD regulation functions described above. For the external regulation strategy (EX), the equilibrium constants of the switching model were set to $K_1^{\mathrm{EX}}([K^+_{ex}]) = K_1^{\mathrm{DUAL}}([K^+_{ex}])$, $K_2^{\mathrm{EX}} = K_2^{\mathrm{DUAL}}(46\ \mathrm{mM})$. For the internal regulation strategy (IN), the autokinase activity the equilibrium constants were $K_1^{\mathrm{IN}} = K_1^{\mathrm{DUAL}}(2\ \mathrm{mM})$, $K_2^{\mathrm{IN}}([K^+_{free}]) = K_2^{\mathrm{DUAL}}([K^+_{free}])$. The constant activity values were chosen such that the activity of the EX and IN variants coincide with the DUAL strategy for an environmental K^+ concentration of 2 mM, which lies within the range of K^+ levels at which induction of *kdpFABC* expression was observed (Fig. 5C).

To study the steady state output of Kdp regulation, the model was again initialized with Dp=Ep=0, $[K^+_{in}]$=250 mM, F=0, V=2×10^{-4}, but now with $\left[K^+_{ex}\right]$ set to the indicated value. The dynamics were then simulated for each of the regulation strategies for a period of 120 hours without depletion of $\left[K^+_{ex}\right]$ or growth ($\frac{d\left[K^+_{ex}\right]}{dt} = \frac{d\mathrm{V}}{dt} = 0$).

To simulate the competition between different regulation strategies, we set up simulations consisting of a copy of the variables $\{\mathrm{Dp}_s, \mathrm{Ep}_s, \mathrm{F}_s, [K^+_{in}]_s, \mathrm{V}_s\}$ together with their associated dynamics for each of the three strategies, $s \in \{\mathrm{DUAL}, \mathrm{EX}, \mathrm{IN}\}$, and a single shared environment $\left[K^+_{ex}\right]$. Simulations were initialized with $\{\mathrm{Dp}_s$=Ep_s=0, $[K^+_{in}]_s$=250 mM, F_s=0,V_s=(2/3)×10$^{-4}\}$ for all strategies in an environment $[K^+_{ex}]$=5 mM and again run for 12 hours with $\frac{d\left[K^+_{ex}\right]}{dt} = \frac{d\mathrm{V}_s}{dt} = 0$. Subsequently growth and depletion of environmental $[K^+_{ex}]$ was re-enabled and the simulation was switched to random environments. We selected a random new $\left[K^+_{ex}\right]$ value from an exponential distribution with parameter λ=(2/ln(2)) mM chosen such that the median concentration equals the point at which the three strategies show matching activities. A new maximal growth rate parameter μ_{max} (common to all strategies) was selected from a uniform distribution over the range 0.25-2 h^{-1}. The duration of this environment was chosen from an exponential distribution with mean τ=90 min. After this amount of simulation time had elapsed a new environment described by a set of $[K^+_{ex}]$, μ_{max} and τ were selected. In addition, in order to keep the cell density manageable, each time that a new environment was generated the total population was re-diluted back to the initial density but maintaining the relative abundance of cells with each strategy, $\mathrm{V}_s \rightarrow \left(\frac{\mathrm{V}_s}{\sum_s \mathrm{V}_s}\right)$×2×10^{-4} for each strategy s.

Supplemental References

Blattner, F. R., G. Plunkett, 3rd, C. A. Bloch, N. T. Perna, V. Burland, M. Riley, J. Collado-Vides, J. D. Glasner, C. K. Rode, G. F. Mayhew, J. Gregor, N. W. Davis, H. A. Kirkpatrick, M. A. Goeden, D. J. Rose, B. Mau & Y. Shao, (1997). The complete genome sequence of *Escherichia coli* K-12. Science *277*: 1453-1462.

Fried, L., J. Lassak & K. Jung, (2012). A comprehensive toolbox for the rapid construction of *lacZ* fusion reporters. J. Microbiol. Meth. *91*: 537-543.

Guzman, L. M., D. Belin, M. J. Carson & J. Beckwith, (1995). Tight regulation, modulation, and high-level expression by vectors containing the arabinose P_{BAD} promoter. J. Bacteriol. *177*: 4121-4130.

Heermann, R., K. Altendorf & K. Jung, (2003). The N-terminal input domain of the sensor kinase KdpD of *Escherichia coli* stabilizes the interaction between the cognate response regulator KdpE and the corresponding DNA-binding site. J. Biol. Chem. *278*: 51277-51284.

Heermann, R., T. Zeppenfeld & K. Jung, (2008). Simple generation of site-directed point mutations in the *Escherichia coli* chromosome using Red®/ET® Recombination. Microb. Cell. Fact. *7*: 14.

Jung, K. & K. Altendorf, (1998b). Truncation of amino acids 12-128 causes deregulation of the phosphatase activity of the sensor kinase KdpD of *Escherichia coli*. J. Biol. Chem. *273*: 17406-17410.

Jung, K., R. Heermann, M. Meyer & K. Altendorf, (1998). Effect of cysteine replacements on the properties of the turgor sensor KdpD of *Escherichia coli*. Biochim. Biophys. Acta *1372*: 311-322.

Kollmann, R. & K. Altendorf, (1993). ATP-driven potassium transport in right-side-out membrane vesicles via the Kdp system of *Escherichia coli*. Biochim. Biophys. Acta *1143*: 62-66.

Nakashima, K., A. Sugiura, K. Kanamaru & T. Mizuno, (1993). Signal transduction between the two regulatory components involved in the regulation of the *kdpABC* operon in *Escherichia coli*: phosphorylation-dependent functioning of the positive regulator, KdpE. Mol. Microbiol. *7*: 109-116.

Narayanan, A., L. N. Paul, S. Tomar, D. N. Patil, P. Kumar & D. A. Yernool, (2012). Structure-function studies of DNA binding domain of response regulator KdpE reveals equal affinity interactions at DNA half-sites. PloS one *7*: e30102.

Rhoads, D. B., F. B. Waters & W. Epstein, (1976). Cation transport in *Escherichia coli*. VIII. Potassium transport mutants. J. Gen. Physiol. *67*: 325-341.

Schlösser, A., M. Meldorf, S. Stumpe, E. P. Bakker & W. Epstein, (1995). TrkH and its homolog, TrkG, determine the specificity and kinetics of cation transport by the Trk system of *Escherichia coli*. J. Bacteriol. *177*: 1908-1910.

Studier, F. W. & B. A. Moffatt, (1986). Use of bacteriophage T7 RNA polymerase to direct selective high-level expression of cloned genes. J. Mol. Biol. *189*: 113-130.

Surmann, K., V. Laermann, P. Zimmann, K. Altendorf & E. Hammer, (2014). Absolute quantification of the Kdp subunits of *Escherichia coli* by multiple reaction monitoring. Proteomics *14*: 1630-1638.